# A combined methodology for reconstructing source-to-sink basin evolution, exemplified by the Triassic Songpan–Ganzi basin, central China

# A combined methodology for reconstructing source-to-sink basin evolution, exemplified by the Triassic Songpan-Ganzi basin, central China

Guohui Chen[1], Fangyang Hu[2,3,4*], Alastair H. F. Robertson[5], Eduardo Garzanti[6], Shaohua Zhang[7], Fu-Yuan Wu[3,7]

1 School of Earth Sciences and Engineering, Hohai University, Nanjing 210098, China

2 Key Laboratory of Mineral Resources, Institute of Geology and Geophysics, Chinese Academy of Sciences, Beijing 100029, China

3 Innovation Academy for Earth Science, Chinese Academy of Sciences, Beijing 100029, China

4 Department of Geosciences, University of Arizona, Tucson, AZ, USA

5 School of GeoSciences, University of Edinburgh, Grant Institute, James Hutton Road, Edinburgh EH9 3FE, UK

6 Laboratory for Provenance Studies, Department of Earth and Environmental Sciences, Università di Milano-Bicocca, Milano 20126, Italy

7 State Key Laboratory of Lithospheric Evolution, Institute of Geology and Geophysics, Chinese Academy of Sciences, Beijing 100029, China

*Corresponding author: Fangyang Hu (hufangyang@mail.iggcas.ac.cn)

**Abstract:** Source-to-sink evolution of basin is a key to understand sedimentary processes, especially in a complex regional orogenic setting. Detrital zircon populations can be traced from their primary sources to their depositional settings. The resulting interpretations are enhanced by calculation of the adjacent orogen's paleoaltimetry, which provide additional insights into paleogeography. In this study, we present a combined methodology which aims to reconstruct source-to-sink evolution by the analysis of detrital zircon age distribution in sandstones, together with the calculation of paleo-elevation of surrounding orogens based on the chemical compositions of coeval magmatic rocks. We test the method using detrital zircon U-Pb geochronology datasets from the Triassic Songpan-Ganzi basin in central China, combined with whole-rock geochemical data from intermediate-composition magmatic rocks in adjacent crustal blocks. Application of the combined methodology supports a syn-collisional basin model for the formation of the Triassic Songpan-Ganzi basin (in preference to a continental back-arc basin). The clastic sediments, mainly deep-marine turbidites, accumulated in a remnant Paleotethyan Ocean that was surrounded by the converging North China Block, South China Block, East Kunlun Orogenic Belt and the Qiangtang Block. The North China Block and the North Qaidam Block were major proto-sources of detrital zircons to the basin, contributing on average 12% and 15%, respectively. Triassic magmatic rocks in the East Kunlun and the Qiangtang regions were major sources of igneous zircons, up to 68% for the former and up to 56% for the latter. Despite being located at a calculated elevation of ca. 4000 m, the Qinling Orogenic Belt contributed only ca. <10% of the zircons, mostly restricted to the eastern depocenter of

45 the basin. In contrast, supply from the North Qiangtang Block, despite its calculated
46 lower elevation (1000-3000 m), accounts for 2-10% of the detrital zircons in the basin,
47 suggesting high erosion rates of this block. The minimal supply of zircons from the
48 South China Block, restricted to 3-6% in the central and western depocenters, is
49 inconsistent with the zircon abundances predicted in the alternative back-arc basin
50 model of the Songpan-Ganzi basin.
51
52 Keywords: detrital zircon geochronology, paleo-elevation, proto-source contribution,
53 provenance, Songpan-Ganzi basin
54
55 **1. Introduction**
56 Sedimentary provenance provides important clues concerning processes of
57 sedimentary deposition, basin sedimentation, hinterland tectonics and exhumation (e.g.,
58 Dickinson and Gehrels, 2003, 2008; Smyth et al., 2014). Detrital minerals has received
59 considerable attention in clastic rock studies as they represent valuable petrogenetic and
60 provenance indicators (e.g., Grigsby, 1990; Mange and Maurer, 1991; Morton, 1991;
61 von Eynatten and Gaupp, 1999; Garzanti and Andò, 2019). Variations in the
62 geochemical composition of detrital minerals relate to the host rocks and so allow the
63 mineralogical signature of the source rocks to be characterized (e.g., Mange and Maurer,
64 1991; Morton and Hallsworth, 1994; Rubatto, 2002; Belousova et al., 2002; Meinhold,
65 2010; Andò et al., 2014).
66 During the last decade, attention has focused on zircon geochronology, which is

widely used to unravel sedimentary provenance, the linkages between different sedimentary units, and the ages of deposition (Fedo et al., 2003; Andersen, 2005; Gehrels, 2011; Vermeesch, 2012; He et al., 2020). The combined use of a Concordia diagram with Isoplot (Ludwig, 2008) and an age-distribution diagram (or relative age probability plot) represent well-established techniques to illustrate and interpret detrital zircon ages (Sircombe, 2004; Sircombe and Hazelton, 2004). Visual methods alone are becoming increasingly difficult to compare large detrital geochronology data sets (e.g., Gehrels, 2000; DeGraaff-Surpless et al., 2003; Fedo et al., 2003; Vermeesch, 2013), mainly because of the large sample sizes and the number of samples (e.g., Saylor and Sundell, 2016). Although provenance can be interpreted by using whole-rock methods such as sediment petrography and chemical analysis, several recently developed methods aid quantification of the proto-source contributions of detrital age distribution. Specifically, the detrital age population unmixing method (Sundell and Saylor, 2017; Clift et al., 2020) helps to identify unknown sources and sedimentary recycling. In addition, paleo-elevations can be derived from intermediate-composition magmatic rocks that are well-dated radiometrically and analyzed chemically and can be used to help interpret tectonic settings and landscape evolution (Airy, 1855; Lee et al., 2015; Hu et al., 2017, 2020a; Zhu et al., 2017). Specifically, empirical relationships have recently been established between the geochemical indices of magmatic rocks and crustal thickness/elevation of mountain belts (Chapman et al., 2015; Profeta et al., 2015; Hu et al., 2017, 2020a; Tang et al., 2021; Luffi and Ducea, 2022). This approach can facilitates the interpretation of paleo-elevation and topographic relief in a potential

source area, allowing a better interpretation on source-to-sink relationships.

In this paper, we provide a general guide to assist readers in interpreting sediment provenance by re-evaluating detrital-zircon age distributions and source correlations, combined with paleo-elevation estimates of surrounding orogens. In order to evaluate the efficiency and applicability of the proposed combined method, we utilize a case study involving detrital zircon geochronological datasets from Triassic sandstones of the Songpan-Ganzi basin. We combine this with whole-rock geochemical data from Permian-Upper Triassic magmatic rocks of both the Songpan-Ganzi basin and the surrounding orogens (e.g., Zhan et al., 2018; Dong et al., 2018; Hu et al., 2020b). The overall results illustrate the value of combining detrital geochronological age distributions and calculated paleo-elevations to help decipher the geological development of Paleotethys within and adjacent to the Songpan-Ganzi basin.

## 2. User's guide to unmixing detrital zircon age distribution

To allow a thorough comparison of detrital data sets, we propose the series of steps shown in Fig. 1a. The weighting of proto-sources (i.e., primary sources) contribution needed to take account of several precautionary aspects, complementary information and available geological interpretation, as explained below.

### 2.1 Step 1: Screening: sample size and age selection

The first step in detrital zircon provenance studies concerns how many detrital zircon grains should be analyzed. The statistics of individual sample indicate that at least 60 grains need to be analyzed to have a 95% probability of identifying individual

111 component that make up at least 5% of the detrital age spectrum (Dodson et al., 1988).
112 By comparison, Vermeesch (2004) calculated that in order to maintain a population
113 proportion exceeding 0.05 of the total population at 95% confidence, a minimal of 117
114 grains should be analyzed, in accordance with the well-known binomial probability
115 formula. Monte Carlo simulation of detrital zircon age populations suggest that the
116 threshold values of sample size are likely to be underestimated if the complexity of
117 zircon populations is fully considered (Andersen, 2005; Gehrels, 2011). Some
118 quantitative statistical methods; e.g., the Kolmogorov-Smirnov (K-S) and Kuiper tests,
119 are closely related to sample size and age distributions, such that very large data sets
120 (n > 300) are usually required for quantitative comparisons (Saylor and Sundell, 2016).
121 In order to improve statistical robustness and analytical accuracy, it is therefore
122 advantageous, where possible, to group samples from basins and formations, thereby
123 increasing the sample size for each specific depositional region and time period (e.g.,
124 Clift et al., 2020).

125 Uncertainties in the ages derived from the laboratory analysis of zircons vary as a
126 function of age (e.g., Ludwig, 2008). In general, interpretations of zircon ages can be
127 selected by $^{206}Pb/^{238}U$ ages for zircon grains < 1000 Ma, and on $^{207}Pb/^{206}Pb$ ages for
128 grains > 1000 Ma (e.g., Gehrels, 2000; Gehrels et al., 2008). The ages were filtered
129 using a ±20% discordance cutoff for zircon <200 Ma, and a ±10% discordance cutoff
130 for zircon >200 Ma. The degree of discordance = a percentage of the $^{206}Pb/^{238}U$ age
131 divided by the $^{207}Pb/^{235}U$ age (or $^{206}Pb/^{207}Pb$ age if zircon >1000 Ma).
132

## 2.2 Step 2: Display detrital zircon age distribution

A simple histogram can be used to illustrate the abundance of grain ages in any particular sample (Machado et al., 1996). This can be illustrated by vertical bars on finite mixture distributions; e.g., in probability density plots (PDPs), or as kernel density estimates (KDEs) (Dodson et al., 1988; Sircombe, 2004; Sircombe and Hazelton, 2004; Ludwig, 2008; Vermeesch and Garzanti, 2015). Detrital age spectra can also be illustrated on cumulative distribution functions (CDFs), with step segments shown in the distribution. CDFs can also be used for statistical comparisons of multiple samples that have different curve slopes and steps. Detailed comparisons, merits and deficiencies of these methods are discussed in Vermeesch (2012), Saylor and Sundell (2016) and Vermeesch and Garzanti (2015).

## 2.3 Step 3: Differences and similarities between samples

It is possible to perform quantitative comparisons of geochronological data using the K-S Test/Kuiper Test (Saylor and Sundell, 2016; Vermeesch et al., 2016). The related statistics, the D factor for the K-S Test and the V factor for the Kuiper Test, respectively, are be calculated from the two CDFs (Saylor and Sundell, 2016). In addition, metrics of Similarity, Likeness and Cross-correlation coefficients are based on either the age distribution of PDPs or the KDEs. Two- or three- dimensional nonmetric multidimensional scaling (MDS) of age distributions provides greater resolution for visual comparison, in which the distance between the sample points represents the degree of divergence between them (Vermeesch, 2013).

155

156 2.4 Step 4: Identify potential sources

157 Potential sources can be used as end-members to help determine the mixing
158 proportions and to interpret the general trends in sediment derivation. It is possible to
159 identify a range of source candidates by observing the characteristics of
160 multidimensional scaling plots, in the light of the regional geology (e.g., Clift et al.,
161 2020). Sediment samples and their potential sources tend to group; e.g., plot between
162 the source end-members in the multidimensional scaling plots. Differences between
163 samples suggest that the region was being supplied from more than one source.

164 Recycling is a common sedimentation processes, which can complicate sample
165 unmixing and is known to affect provenance interpretation (Gehrels, 2011; Garzanti et
166 al., 2013). In order to quantify provenance changes, systematic major changes in the
167 zircon age population need to be identified, bearing in mind that even apparently unique
168 peaks in the zircon distribution can be recycled from older sediments.

169

170 2.5 Step 5: Source unmixing and relative contributions (Monte Carlo Mixture
171 modelling)

172 Mixing proportions for source samples can be determined by using the inverse
173 Monte Carlo and forward optimization methods that compare the samples to possible
174 source end-members (e.g., Sundell and Saylor, 2017). The computational model can be
175 easily accessed via a MATLAB-based file (e.g., Sundell and Saylor, 2017). This
176 software tests uncertainty by randomly generating different source contributions. For

177 quantitative comparison, various statistics can be used; e.g., the K-S test D and Kuiper
178 test V values of CDFs, and the Cross-correlation coefficient of PDPs or KDEs (Sundell
179 and Saylor, 2017).

180 The modelled output patterns are similar to the input age patterns, allowing the
181 relative contributions from different sources to be calculated (Sundell and Saylor, 2017).
182 Where the analyzed zircon distributions fall close to the model range, the source
183 proportion estimates may be considered well found. On a statistical basis, large detrital
184 geochronological data sets, preferably from numerous samples, provide robust
185 confidence levels and also aid quantitative inter-sample comparisons (Saylor and
186 Sundell, 2016; Sundell and Saylor, 2017). In addition, a larger sample size allows for
187 effective and precise rejection of the null hypothesis; i.e., that the two data sets have
188 the same distribution, due in part to the perturbation of the random sampling of 'big
189 data' (Saylor and Sundell, 2016).

190 Although source unmixing can quantitatively represent the geochronological
191 features of samples, precautions should be taken when interpreting e.g., zircon fertility,
192 zircon recycling, and sorting behavior (e.g., Malusà and Garzanti, 2019; Clift et al.,
193 2020). Notably, samples can be modelled better if they have a larger sample size (Saylor
194 and Sundell, 2016; Sundell and Saylor, 2017), which can be achieved by grouping
195 samples that have similar depositional ages or geographic localities.

196

197 **3. User's guide to paleo-elevation estimates**

198 3.1 Step 1: Synthesis of regional magmatic rock data

Variations in paleo-elevation can help to understand the relationship between tectonic processes and landscape evolution. The recently developed paleoaltimetry technique (Chapman et al., 2015; Profeta et al., 2017; Hu et al., 2017, 2020a) that is applied here uses the whole-rock geochemistry of intermediate-composition magmatic rocks from subduction and/or collision zones to estimate quantitatively the early-growth of topography at convergent margins. The calculation of paleo-crustal thicknesses and paleo-elevation assume Airy isostatic equilibrium (Airy, 1855; Lee et al., 2015; Hu et al., 2017; Zhu et al., 2017). When magma is formed by melting and fractionation within thick crust (>1.0 GPa), Y and Yb are incorporated into garnet and amphibole, whereas Sr and La remain in the liquid leading to increased Sr/Y and $(La/Yb)_N$ in the magma (i.e., chondrite-normalized values) (after McDonough and Sun, 1995). In contrast, for magma derived from melting and fractionation of normal-thickness or thinned crust (<1.0 GPa), Sr is incorporated into plagioclase, whereas Y and Yb remain in the liquid, resulting in magma with low Sr/Y and $(La/Yb)_N$ ratios. Therefore, the trace element ratios [Sr/Y and $(La/Yb)_N$] of the intermediate magmatic rocks represent related proxies that can be used to indicate the crustal thickness, and by extension, the paleo-elevation of collisional belts and magmatic arcs. This method has been successfully applied in Iran (Chaharlang et al., 2020; Moghadam et al., 2022), the Tibetan Plateau (Zhan et al., 2018; Hu et al., 2020a; Sundell et al., 2021), the Colombian Andes (León et al., 2021), the Rocky Mountains (Lipman, 2021), and the Appalachian orogen (Hillenbrand and Williams, 2021).

The regional geological information and available analyzed data of suitable

magmatic rocks of the relevant basin, its surrounding cratons and orogenic belts should next be compiled, followed by further screening (Fig. 1b).

### 3.2 Step 2: Screening, data filtered and paleo-elevation reconstruction

Samples that were formed by partial melting, assimilation, or fractional crystallization processes at shallow crustal levels (<1.0 GPa) are generally unsuitable for true crustal thickness/paleo-elevation estimates (Chapman et al., 2015; Hu et al., 2017) and should be excluded from the data compilation. Accordingly, for magmatic rocks formed during oceanic subduction, the samples should be filtered with $SiO_2$ = 55-70 wt%, MgO = 1.0-6.0 wt%, and Rb/Sr < 0.20, according to the protocols of Chapman et al. (2015). By comparison, filtered samples of magmatic rocks that were emplaced during the transition from oceanic subduction to continental-collision or in continental-collision setting are characterized by $SiO_2$ = 55-72 wt%, MgO = 0.5-6.0 wt%, and average Rb/Sr < 0.35 (Hu et al., 2020a), eliminating the effects of highly fractionated rocks (Chapman et al., 2015). In addition, the high La (>70 ppm) samples from collisional settings are also excluded from the compilation because La content can strongly increase during potential high-temperature melting (Hu et al., 2020a). This increase could cause the relatively high La/Yb ratios and as a result lead to inaccurate paleo-elevation calculations (Hu et al., 2020a). Sr/Y and $(La/Yb)_N$ ratios were processed and filtered by following a modified Thompson Tau method (Hu et al., 2020a). The outliers mentioned above were then excluded from the paleo-elevation calculations and the resulting contour graphs. Explanations and limitations of the

243 method are noted by Hu et al. (2020a).

244 The paleo-elevations of surrounding orogens/mountain belts were calculated here
245 according to the empirical equations of Hu et al. (2020a). The elevations of subduction
246 zones and collisional zones tend to correlate positively with crustal thicknesses when
247 calculated using several different empirical equations (Hu et al., 2020a). The related
248 data were then used to plot a contour map of the study area using SURFER software.
249 The quantitatively constrained paleo-altitude/crustal thickness of the selected region
250 becomes more accurate according to the number of data points available.

251

252 **4. Selected case history: the Triassic Songpan-Ganzi basin**

253 Here, we take the classic geological region of the Songpan-Ganzi basin in central
254 China as an example, to test the applicability and effectiveness of our approach to
255 quantify detrital zircon age spectra and paleo-elevation estimates. Sandstones of Early
256 to Late Triassic age are exposed in the Songpan-Ganzi basin, which relate to the Late
257 Paleozoic-Early Mesozoic geological evolution of the eastern Paleotethys (Fig. 2) (Yin
258 and Nie, 1993; Nie et al., 1994). The Triassic sandstones of this region have already
259 been extensively studied in terms of sedimentology, petrography and geochemistry (e.g.,
260 Gu, 1994; Zhou and Graham, 1996; She et al., 2006; Zhang et al., 2008, 2012; Ding et
261 al., 2013). Numerous efforts have been made to understand the spatial and temporal
262 provenance characteristics of these Triassic deposits using detrital zircon
263 geochronology (Bruguier et al., 1997; Weislogel et al., 2006; Enkelmann, et al., 2007;
264 Weislogel, 2008; Ding et al., 2013, Jian et al., 2019; Tang et al., 2023; Pan and Hu,

2023).

Two main tectonic hypotheses have been proposed for the geological setting of the Songpan-Ganzi basin (Fig. 3). In the first hypothesis (syn-collisional basin model) (Fig. 3a), the Songpan-Ganzi basin is interpreted as part of the north-easternmost branch of Paleotethys (e.g., Stampfli and Borel, 2002), which evolved from a remnant-ocean basin into a collisional orogenic belt (e.g., Sengör, 1987; Yin and Nie, 1993; Ingersoll et al., 1995; Zhou and Graham, 1996; Chang, 2000; Tang et al., 2022). In this interpretation, the sedimentary provenance was intimately related to the collision of the South China Block and the North China Block. In the second hypothesis, a back-arc rifting setting is proposed (Fig. 3b), in which the western part of the Songpan-Ganzi basin (Hoh-Xil area) was supplied from both the North and the South China blocks (Ding et al., 2013). In this interpretation, detritus was transported along the western margin of the South China Block, mixed, and then accumulated within the westernmost part of the Songpan-Ganzi Basin (Ding et al., 2013).

To support, our case study of the Songpan-Ganzi basin, numerous geochemical data exist for the magmatic rocks in the surrounding orogens, which represent potential source rocks for the Songpan-Ganzi basin (e.g., Dong et al., 2018; Lu et al., 2019; Hu et al., 2020b).

Our case study of the Songpan-Ganzi basin sandstones aims to achieve the following: (1) to compare multiple detrital zircon data sets of sandstones throughout the Songpan-Ganzi basin; (2) to quantitatively determine the relative provenance contribution of their crustal proto-sources; (3) to shed light on the paleo-elevation and

topographic evolution of the source area; and (4) to determine the potential for alternative controls on the age spectrum of detrital zircons associated with the tectonic evolution of the Songpan-Ganzi basin and the eastern Paleotethys.

### 4.1 Summary geology of the Songpan-Ganzi basin

The Songpan-Ganzi basin is distinguished by extremely thick Triassic sediments (c. 8 km) (Enkelmann et al., 2007), which relate to the closure of Paleotethys (Ding et al., 2013; Jian et al., 2019; Wu et al., 2020). The Songpan-Ganzi basin is separated from the East Kunlun and Qinling Orogenic Belts by an ophiolitic mélange belt, termed the A'nyemaqen-Mianlue suture zone (e.g., Dong et al., 2018; Hu et al., 2020b) (Fig. 2). During the Late Paleozoic to Early Mesozoic, Paleotethyan oceanic lithosphere was being subducted northward along the E-W-trending active margin now represented by the East Kunlun and Qinling Orogenic Belts (Fig. 2). Paleotethys in this region closed during Middle to Late Triassic times (Dong et al., 2018; Kapp and DeCelles, 2019; Wu et al., 2019; Hu et al., 2020b). In addition, the Songpan-Ganzi basin is separated from the Qiangtang Block by a wide belt of Permian-Triassic sedimentary mélange belonging to the Jinshajiang suture zone (Fig. 2), which is interpreted as a Paleotethyan subduction complex (Kapp et al., 2000, 2003; Pan et al., 2004; Pullen et al., 2008; Kapp and DeCelles, 2019).

The basement of the Songpan-Ganzi basin consists of continental crust which is generally correlated with the South China Block (e.g., Wang et al., 2016; Wu et al., 2019; Hu et al., 2022). Following earlier subduction, remnant Paleotethyan oceanic

crust was emplaced onto the crust of the South China Block/Qiangtang Block as a consequence of late-stage oceanic subduction and subsequent continental collision, specifically the convergence between the Qiangtang Block and South China Block with Eurasia (Dong et al., 2018) (Fig. 3). Thick Triassic turbidites that had accumulated within the Songpan-Ganzi basin were progressively deformed as a result of the collision of the adjacent blocks (e.g., Faure et al., 2001; Kirby et al., 2002; Roger et al., 2003, 2011; Meng et al., 2019). The basin uplifted during the Late Triassic (Norian), as indicated by a switch from deep-sea turbidites to deltaic deposits (Bureau of Geology and Mineral Resources Sichuan Province [BGMRSP], 1991; Chang, 2000). During the Late Triassic, southeastward thrusting occurred along the western margin of the South China Block, forming the Longmen-Shan thrust belt and causing deformation of the Sichuan Basin to the east (Burchfiel et al., 1995) (Fig. 2).

The Lower to Upper Triassic sandstones of the Songpan-Ganzi basin discussed here accumulated during the closure of Paleotethys from oceanic subduction to continental collision. In addition, widespread magmatism during the Late Triassic inferred post-collisional stage generated widespread granitic intrusions within the Upper Triassic strata of the Songpan-Ganzi basin.

### 4.2 Sampling and data analysis

Published detrital-zircon populations of 63 sandstone samples were selected for inverse Monte Carlo modeling, namely from the northeastern (19), southeastern (9), central (19), and western (16) depocenters (Figs. 4-5). In order to increase sampling

density and more fully evaluate the relationship between the Songpan-Ganzi basin and the potential proto-sources, a newly analyzed data subset (n=7) from the southeast of the basin was compiled in the data analysis.

The newly collected sandstone samples (n=7) from the southeast of the basin (Fig. 4) were crushed and sieved. Zircons were separated using standard elutriation and magnetic separation techniques (e.g., McLennan et al., 2001). The zircons were picked by hand using a binocular microscope, embedded in epoxy resin, and polished. U-Pb dating of zircons was conducted in situ using an Agilent 7500a Quadrupole-Inductively Coupled Plasma Mass Spectrometry (ICP-MS), coupled with a GeoLasHD 193 nm ArF excimer laser ablation system at the Institute of Geology and Geophysics, Chinese Academy of Sciences. The analytical procedure is explained in Xie et al. (2008). In this study, a laser beam diameter = 32 μm, energy density = 4 J $cm^{-2}$, and frequency = 5 Hz were used. Zircon standard 91500 was used for calibrating the U-Pb fractionation; its $^{207}Pb/^{206}Pb$ age is 1065.4 ± 0.3 Ma (Wiedenbeck et al., 1995). The second reference zircon SA01 with a $^{206}Pb/^{238}U$ age of 535.08 ± 0.32 Ma (Huang et al., 2020) was used to monitor accuracy. In addition, the GLITTER software (GEMOC, Macquarie University; Griffin et al., 2008) was used for calibrating the raw data. Common lead corrections were performed following the method detailed by Andersen (2002). The complete dataset is provided in the Supplementary Table S1.

Geochronological ages are summarized for the Permian to Triassic magmatic rocks in the Qinling and Qiangtang regions in Supplementary Table S2. In addition, geochemical data were compiled for Upper Permian to Upper Triassic magmatic rocks

353 from the Songpan-Ganzi basin, the East Kunlun Orogenic Belt, the Qinling Belt, and
354 the North Qiangtang Block (Supplementary Table S3-S4). Paleo-elevations were
355 calculated for each of these potential source-rock domains based on these complied data
356 by using the method presented above (Supplementary Table S3). For the margin of the
357 Songpan-Ganzi basin, the paleo-elevation, closely related to water depth, was also
358 estimated based on the sedimentary facies/fabrics and related fossil species (e.g., Chang,
359 2000).
360
361 4.3 Regional depocenters
362 The Triassic sedimentary rocks in the Songpan-Ganzi basin show significant
363 spatial and temporal variations in lithology, sediment composition and facies (She et
364 al., 2006; Weislogel, 2008; Zhang et al., 2008, 2012). Four main depocenters (Fig. 5)
365 can be recognized based on facies variation, paleocurrent data (Weislogel et al., 2006;
366 Ding et al., 2013; Jian et al., 2019) and restored Triassic isopachs (after Wang and Pan,
367 2010; Zhang et al., 2019).
368 The northeastern depocenter is likely to extend across the western South Qinling
369 Belt and the south of the Mianlue-A'nyemaqen Suture (Fig. 5a). The Triassic sequence
370 thickens westwards, reaching ca. 6 km (Wang and Pan, 2010; Zhang et al., 2019).
371 Southwesterly paleocurrents dominate (Weislogel et al., 2006; Ding et al., 2013),
372 whereas average grain size decrease westwards (Chang, 2000). The lithofacies change
373 westwards from neritic/bioclastic limestone to mixed calciclastic-siliciclastic marine
374 turbidites (Zhou and Graham, 1996; Weislogel, 2008; Weislogel et al., 2010),

375 suggesting deepening in this direction.

376 The southeastern depocenter thickens westwards from the present Longmen Shan
377 Thrust Belt to the Ganzi-Litang area (Fig. 5b), culminating in ca. 7 km of Triassic strata
378 (Wang and Pan, 2010; Zhang et al., 2019). This depocenter is characterized by northerly
379 paleocurrents (Ding et al., 2013; Jian et al., 2019) and an abundance of metamorphic
380 lithic grains (Chen et al., 2006; Su et al., 2006; Zhang et al., 2012). The lithologies
381 change northwards from dominantly calciclastics to siliciclastics (Weislogel, 2008).

382 The central depocenter is restricted to the Maduo-Maqin-Maqu-Ganzi-Yushu area
383 (Fig. 5c). Paleocurrent orientations are variable, ranging from north/northwest to
384 south/southwest (Ding et al., 2013; Jian et al., 2019).

385 The western depocenter, by far the largest, extends from the eastern Maduo-Yushu
386 area to the western Hoh-Xil area (Fig. 5d). The sediments in this region display opposite
387 paleocurrent directions (Ding et al., 2013).

388

389 **5. Application of the combined method to the Songpan-Ganzi basin**

390 We first performed the stepwise evaluation and interpretation, in line with the
391 methodology explained above (see Section 2-3). The geochronological data pass the
392 initial verification phase; i.e., samples with geographical proximity are pooled together
393 to increase sample size; the ages are filtered and illustrated using the same criteria (see
394 Section 2.1) (Fig. 1). The whole-rock geochemical data for magmatic rocks of suitable
395 intermediate composition were then filtered (Supplementary Table S4) in order to
396 eliminate data subsets with undefined petrogenesis (see Section 3.2), following the

protocols of Chapman et al. (2015).

5.1 Geochronology age spectra

The Kernel Density Estimation (KDE) best captures the distribution of data with high quality (precision) or quantity (number of analyses) (Vermeesch, 2012) (Fig. 6).

For all of the samples considered (n=63), those from the northern depocenter (Fig. 5) contain abundant Paleoproterozoic (1700-2000 Ma) and Archean (2400-2600 Ma) zircons, together with Paleozoic populations, peaking at 270 Ma, 330 Ma, and 440 Ma (Supplementary Fig. S2) (Fig. 6). Samples from the southern depocenter (Fig. 5) yielded age populations with a notable Neoproterozoic peak and variable Triassic, Ordovician-Devonian, Paleoproterozoic and Archean clusters (Weislogel et al., 2006; Ding et al., 2013) (Supplementary Fig. S3) (Fig. 6). Samples from the central depocenter (Fig. 5) define five populations, namely 240-310 Ma (Late Carboniferous-Early Triassic), 400-480 Ma (Ordovician-Early Devonian), 750-1000 Ma (Tonian), 1700-2000 Ma (Late Paleoproterozoic) and 2300-2600 Ma (Neoarchean-Early Paleoproterozoic) (Jian et al., 2019) (Supplementary Fig. S4) (Fig. 6). Samples from the western depocenter (Fig. 5) have variable age signatures, including relatively young 480-400 Ma and 300-200 Ma populations (Supplementary Fig. S5) (Fig. 6). Neoproterozoic grains dated from 750 Ma to 1030 Ma are locally present and Paleoproterozoic and Archean zircons also occur.

5.2 Statistical comparisons of detrital zircon geochronology

To compare the potential sources of the early Mesozoic with the older components,

419 the compiled ages were filtered to include only grains >227 Ma; i.e., ages prior to the
420 known uplift of the Songpan-Ganzi basin, which resulted from tectonically controlled
421 shallowing (e.g., Zhan et al., 2018; Tang et al., 2018). This filter also reduces bias in
422 statistical analyses shat would have resulted from the inclusion of younger grains (e.g.,
423 <227 Ma arc magmatics). An existing non-metric multi-dimensional scaling (MDS)
424 map was adapted to compare visually detrital zircon age spectra (Vermeesch, 2013).
425 Samples with similar age spectra plot close to each other on the MDS map, whereas
426 samples with different spectra plot far apart. A multi-dimensional scaling plot based on
427 K-S statistical analysis of the 63 samples from the Songpan-Ganzi basin indicates two
428 major clusters, one related to the major orogenic basement to the left of Figure 7; e.g.,
429 North China Block, South China Block and North Qiangtang Block; these are
430 interpreted as major sources of the detrital zircons. The other cluster is related to the
431 magmatic rocks to the right of Figure 7; this is interpreted to indicate that Qiangtang,
432 Qinling and Kunlun magmatic rocks represent the main sources of the igneous zircons.
433 However, individual samples from different locations vary greatly in the multi-
434 dimensional scaling plots (Fig. 7), which could be explained by the effects of recycling.
435 Therefore, in order to identify similar sediments within the various depocenters, we
436 grouped similar samples within the same depocenter in order to increase sample size
437 and improve statistical accuracy (see Section 2.1), we then used the DZStats program
438 (Saylor and Sundell, 2016) to generate various statistical relationships between the
439 detrital zircon U-Pb age distributions of samples and the potential source candidates
440 (Supplementary Table S5).

441 Following the above statistical analysis, several groups of samples were then
442 clearly recognized as well-separated, effective characterizing different source
443 contributions (Fig. 8). Samples from the northeastern and southeastern depocenters
444 identify as three groups in each area (Fig. 8a-b). On the MDS map (Fig. 7c-d), three
445 groups of age similarities are also recognizable. The northeastern depocenter samples
446 are quite similar to the sediments from the southeastern and western depocenters, and
447 to a lesser extent to the central depocenter (Supplementary Table S5). Group 2 of the
448 northeastern depocenter is particularly similar to many of the samples from the other
449 depocenter; e.g., group 1, 3 of the central depocenter and group 3 of the western
450 depocenter (Supplementary Table S5). The southeastern depocenter (group 3) shows
451 the poorest commonality (Supplementary Table S5; Fig. 7) although this is insignificant
452 because only one sample was analyzed (2003T185; n=95 grains). The Kuiper test
453 necessitates the use of sufficiently large sample sizes (n>300) in order to effectively
454 reject the null hypothesis (e.g., Saylor and Sundell, 2016). The zircon spectrum
455 identified in the southeastern depocenter (group 2) exhibits distinctive characteristics,
456 with notable zircon populations of 200-300 Ma and 360-500 Ma, which, in turn, suggest
457 a different zircon source (Fig. 6). Also, the samples from the central depocenter show
458 the least similarities with the other depocenters (Fig. 7), suggesting that they represent
459 another different sedimentary provenance. The zircon spectrum of the western
460 depocenter is closely comparable with sediments from the north/southeastern
461 depocenter, but to a lesser extent with the central depocenter (Fig. 7). Group 1 of the
462 western depocenter shares great similarities with that of group 2/3, group 2 and group

463 1 of the northeastern, southeastern and central depocenters (Supplementary Table S5).

464

465 5.3 Potential source rock identification

466 The scatterplot of the distances in the MDS plot also points to source correlations
467 (Fig. 7). The zircon populations from the North China Block are closely related to those
468 of the northeastern (e.g., sample 2004T052) and the central (e.g., samples 13SG-62,
469 2004T030 and 2004T013) depocenters (Supplementary Figure S2, S4). Sediments from
470 the western depocenter; e.g., medium-grained sandstones 2007K395, 2005K117 and
471 2005K093 containing monocrystalline quartz, plagioclase and limestone lithics (Ding
472 et al., 2013) are not far apart from the South China Block compositions. Sample
473 2003T185 from the southeastern depocenter (group 3) is a coarse-grained sandstone
474 consisting of plagioclase, monocrystalline quartz, muscovite and limestone lithic grains
475 (Ding et al., 2013). This sample is completely different from the other sandstones based
476 on detrital zircon age population (Supplementary Figure S3), and, as such, was probably
477 fed from local sources (Yidun Terrane-related) (Figs. 6-7).

478 There are a large number of samples with closely related zircon populations, as
479 indicated by their clustering on the MDS map (Fig. 7); e.g., 02MTZ1, 2005K094 and
480 14SSG-24. Given their proximity (Fig. 7), most of these are likely to have been sourced
481 from the North Qiangtang Block, the North Qinling Belt, the eastern/western South
482 Qinling Belt and/or the East Kunlun Orogenic Belt. Notably, the North Qaidam Block-
483 related source fall in the middle of the samples studied (Fig. 7), indicating a provenance
484 relationship. In addition, the zircon populations of the Qiangtang, Kunlun and Qinling

485 magmatic rocks plot to the right of the MDS plot (Fig. 7), indicating a potential source
486 correlation for these samples e.g., 18BPG20, 2007K420 and 2004T286.
487
488 5.4 Source unmixing
489 The highly variable zircon populations of the sandstone turbidites have poorly
490 constrained, generally Triassic depositional ages (e.g., Ding et al., 2013). For these
491 reasons, we carried out the mixing analysis by increasing the sample size via grouping
492 the samples with similar zircon populations (Fig. 8), as recently used by Tang et al.
493 (2023). However, the resulting output is still a poor fit to the model age distribution
494 (i.e., a maximum cross-correlation $R^2$ value =<0.6). This discrepancy can be explained
495 by the mixed sample age distribution of the grouped samples. In order to match the
496 observed zircon age spectrum better, 10,000 attempts were made to replicate a specific
497 (target) detrital age spectrum by varying the contributions from different sources and
498 then selecting the best 1%. The calculated contributions are based on several statistics;
499 i.e., the V statistic of the Kuiper test and D statistic of the K-S test for CDFs, together
500 with the Cross-correlation coefficient for KDEs (Table 1).
501 For the northeastern depocenter, the North China Block (18.3%-21.4%) and the
502 North Qaidam (24.2%-32.8%) constitute the major source contributors for the group 1
503 samples (Table 1). Group 2 samples are characterized by various sources from the East
504 Kunlun magmatic rocks (8.7%-67.9%) and the North Qaidam Block (2.4%-39.7%). In
505 contrast, group 3 samples indicate prominent derivation from the East Kunlun and/or
506 the Qiangtang magmatic rocks (Fig. 9) (Table 1).

For the southeastern depocenter, (1) the cratonic basements of the North China Block, the North Qaidam Block, the South China Block and the western South Qinling Belt; (2) the East Kunlun and Qiangtang magmatic rocks; and (3) the Yidun Terrane/South China Block separately represent the dominant source contributors for group 1, 2 and 3 samples (Table 1).

For the central depocenter, the East Kunlun Orogenic Belt (8.1%-11.8%) and the East Kunlun magmatic rocks (10.5%-50.1%) constitute the dominant sources for group 1 (Table 1), together with a contribution from the North Qaidam Block (5.0%-48.7%). In contrast, the zircon distributions of group 2 mainly relate to the North China Block (33.6%-39.6%) and the North Qaidam Block (17.1%-20.4%). For group 3, the North Qaidam (10.4%-26.8%), East Kunlun (15.1%-23.0%) and Qiangtang (14.6%-40.7%) magmatic rocks represent the main source contributors (Table 1).

For the western depocenter, the model result shows that group 1 samples were derived from the North China Block (20.2%-25.5%), the North Qaidam Block (12. 8%-18.1%), the western South Qinling Belt (ca. 12%) and the north Qinling Belt (9.0%-18.3%) (Table 1). The East Kunlun magmatic rocks (11.8%-19.2%) and the North China Block (32.7%-37.4%) also constitute major zircon sources for the group 2 samples. In contrast, the East Kunlun (11.2%-20.1%) and the Qiangtang (22.2%-47.8%) magmatic rocks constitute major zircon sources only for group 3 samples (Table 1).

### 5.5 Paleo-elevation reconstruction

The closure of the Paleotethys in western China and the formation of the East

529 Kunlun-Qinling orogenic belt were completed by the end of the Triassic (Dong et al.,
530 2018; Hu et al., 2020b). However, how and when these mountain belts were uplifted
531 and provided detritus to the surrounding region is still poorly constrained. The time
532 when the Songpan-Ganzi basin was uplifted high enough to stopped receiving sediment
533 from surrounding orogens is also not well known. Paleo-elevation data for the Songpan-
534 Ganzi basin and its surrounding orogens could therefore greatly aid the regional
535 interpretation.

536 According to our paleo-elevation calculation (Fig. 10), the altitude of the East
537 Kunlun Orogenic Belt increased continuously from Permian to middle Norian (ca. 210
538 Ma) time. Specifically, the East Kunlun Orogenic Belt is inferred to have risen from
539 1000-2000 m to 4000-5000 m before the Rhaetian. Such a high elevation is supported
540 by rapid exhumation of the East Kunlun Orogenic Belt and coarse alluvial (molasse)
541 sedimentation during the Late Triassic (Mock et al., 1999; Jolivet et al., 2001; Liu et al.,
542 2005; Dai et al., 2013; Liu et al., 2020). The marked increase in paleo-elevation of the
543 East Kunlun Orogenic Belt is attributed to regional compressive stress and magmatism
544 during continental collision (Zhu et al., 2017; Dong et al., 2018; Yu et al., 2020).

545 The North Qinling Belt and South Qinling Belt appear to have experienced
546 different paleo-elevation trends. The paleo-elevation of the North Qinling Belt during
547 the Triassic is calculated to have remained constant at ~4000 m, perhaps because the
548 altitude was a consequence of the previous collision of the North and the South Qinling
549 Belts during the Paleozoic (Dong and Santosh, 2016; Hu et al., 2020b). In contrast,
550 during the Middle to Late Triassic, the South Qinling Belt apparently experienced

551 gradually increasing paleo-elevation from ~3000 m to 6000 m, followed by a
552 decreasing of paleo-elevation to ~3000-4000 m (Fig. 10). These paleo-elevations are
553 consistent with the calculated paleo-Moho depths for this orogenic belt (Hu et al., 2017).
554 The significant elevation of the South Qinling Belt is consistent with evidence of
555 thickened continental crust (Hu et al., 2020b). The absence of coeval, Upper Triassic
556 strata in this region (Yang et al., 2021) suggests that significant erosional process took
557 place following surface uplift. The resulting detritus began to supply adjacent basins
558 within the southern North China Block during the Late Triassic (Yang et al., 2021). The
559 above-mentioned decrease in elevation could also be explained by crustal subsidence
560 between the South and North China blocks, possibly triggered by slab break-off and
561 regional delamination resulting from continental collision (Hu et al., 2020b).

562 Relevant data from the northern Qiangtang Block are relatively scarce. From
563 Permian to Carnian times, the topographic elevation of the northern Qiangtang Block
564 is calculated to have been between 1000m and 3000m, without an obviously increasing
565 trend. The paleo-elevation of the northern Qiangtang Block was only about half that of
566 the East Kunlun-Qinling orogenic belt. This relatively modest paleo-elevation is
567 consistent with sedimentological and tectonic records from the northern Qiangtang
568 Block, especially shallowing-upwards of the basin and evidence of terrestrial erosion
569 (Wang et al., 2022). The northern Qiangtang Block has been interpreted as a Lower
570 Triassic foreland basin that formed during continental collision, while a remnant
571 Paleotethys still lay to the south (Fig. 3), followed by uplift above the sea level during
572 Late Triassic time (Wang et al., 2022).

573 The magmatic rocks within the Sonpan-Ganzi Basin are mainly Late Triassic in
574 age (e.g., Zhan et al., 2018). The reconstructed paleo-elevation based on the whole-rock
575 geochemical data for the magmatic rocks cutting the basin (see Section 3.2) are
576 compatible with a broad uplift trend (Fig. 10), with estimated elevations ranging from
577 ca. 3000 m to 6000 m. Such a high elevation is consistent with geophysical and
578 geological evidence, including a thickened crust (~55 km; Zhan et al., 2018) and
579 contemporaneous compressional deformation (e.g., thrusting and folding) during the
580 Late Triassic (Chang, 2000), and also the lack of Jurassic strata in the Songpan-Ganzi
581 basin (Ding et al., 2013). The Upper Triassic magmatic rocks of the Songpan-Ganzi
582 basin intruded these Upper Triassic strata of the basin, showing that sedimentation was
583 completed prior to this magmatism. During the Late Triassic, the uplifted Songpan-
584 Ganzi basin potentially acted as a source for the Upper Triassic strata of the western
585 Sichuan Basin (Yan et al., 2019), consistent with a relatively high elevation by this time.
586

587 **6. Significance for geological development**

588 Integration of our synthesized analysis of detrital zircon contributions and our
589 calculated paleo-elevations, allow us to quantify the proto-source contributions from
590 different crustal basements and/or magmatic rocks; this then facilitates understanding
591 of source-to-sink relationships. Several alternatives have been proposed for sediment
592 provenance in and around the Triassic Songpan-Ganzi basin, in the light of two main
593 plate tectonic hypotheses; i.e., syn-collisional basin or back-arc basin (see Section 4).
594 (1) Multiple deposystems within the Songpan-Ganzi basin were supplied by multiple
595 sources (Weislogel et al., 2006; Tang et al., 2023); (2) the Qinling Orogenic Belt

596 represents the major source of the Songpan-Ganzi basin (Weislogel et al., 2006, 2010;
597 Enkelmann et al., 2007; Gong et al., 2021), together with a possibly rare (Enkelmann
598 et al., 2007) or more significant detrital contributions from the ultrahigh-pressure
599 terrane of the Dabie Orogen farther east (Nie et al., 1994; Weislogel et al., 2010) (Fig.
600 2); (3) the South China Block source dominated only the southeastern depocenter (Ding
601 et al., 2013; Gong et al., 2021); (4) the East Kunlun Orogenic Belt supplied the western
602 depocenter (Enkelmann et al., 2007; Ding et al., 2013) and also the central depocenter
603 (Jian et al., 2019); (5) Supply from the Qiangtang Block dominated the southwestern
604 depocenter (Ding et al., 2013) and/or the more easterly parts of the basin (Gong et al.,
605 2021); (6) whatever the sources, deposition in the basin as a whole continued until the
606 Early Norian (Gong et al., 2021) or Late Norian (Weislogel et al., 2006, 2010;
607 Enkelmann et al., 2007; Ding et al., 2013; Jian et al., 2019). The above very large
608 number of alternative interpretations of the basin's provenance highlight the difficulties
609 of using conventional methods to determine the provenance (e.g., facies, paleocurrents,
610 petrography).

611 Our calculated proto-source proportions (Table 1) suggest by contrast that zircon
612 grains were widely distributed across all of the four depocenters (Fig. 5); i.e., derived
613 from the cratonic basement of the North China Block and the North Qaidam Block,
614 together with magmatic zircons from East Kunlun and the Qiangtang regions (Figs. 2,
615 7; Table 1) (see Section 5.4). This suggests an intimate relationship between the
616 colliding crustal blocks bordering the basin and the resulting Triassic sediments (e.g.,
617 Zhang et al., 2012), as opposed to a dominant contribution from the Qinling-Dabie
618 Orogen (Figs. 2-4) (Nie et al., 1994; Weislogel et al., 2006). Contributions from the
619 Qinling Orogenic Belt proto-source are considered to be low (1.8%-18.3%; Table 1)
620 and do not represent a major source for the basin (Weislogel et al., 2006, 2010;

621 Enkelmann et al., 2007; Gong et al., 2021). Although the Qinling Orogenic Belt
622 apparently reached a high elevation (see Section 5.5; Supplementary Table S3),
623 relatively less detritus from this source (Table 1) is documented in the Songpan-Ganzi
624 basin. Topographic barriers may have separated the Qinling Orogenic Belt from the
625 basin (Yan et al., 2016; Li et al., 2017), although additional evidence (e.g., facies
626 distribution) would be needed to test this. In addition, the concentration of rare metal
627 elements (e.g., Li) in the sandstones of the eastern depocenter is similar to that within
628 intermediate-felsic rocks in the Qinling Orogenic Belt (Hu et al., 2022). The Qinling-
629 derived debris (e.g., zircons) in the western depocenter is mainly documented during
630 the Late Triassic (Ding et al., 2013; Table 1). One option is that this detritus originated
631 in the eastern depocenter and was subsequently incorporated into the western
632 depocenter as a result of sediment recycling during convergence and collision of the
633 Qiangtang and South China blocks with Eurasia. Axial transport to the Songpan-Ganzi
634 basin from the Qinling-Dabie orogenic belts (Figs. 2-3) via orogen-parallel routes (Fig.
635 10) (Weislogel et al., 2006) seems to have been insignificant.

636 The South China Block was a significant contributor to the southeastern depocenter,
637 accounting for, on average, ~15.0% of zircon grains (Table 1). It was also a minor
638 contributor to the central and western regions, averaging 3.4% and 5.8%, respectively
639 (Table 1). The back-arc basin model envisages westward transport of detritus from the
640 continental hinterland of the back-arc basin, represented by the western margin of the
641 South China Block (Ding et al., 2013). Clastic sediments would therefore be expected
642 to decrease in volume and overall grain size in a westerly direction. Also, the relatively
643 proximal sediments in the east should have a prominent South China Block-affinity in
644 the zircon distribution. In reality, there are abrupt changes and variation in zircon
645 abundances between the eastern and the westerly parts of the basin that differ from the

646 expected patterns in the back-arc basin model. However, these features are fully
647 consistent with the preferred continental collision model.

648 The similarities of zircon populations of > 700 Ma in both the South Qinling Belt
649 and the South China Block suggest that the zircons found in the South China Block,
650 previously believed to have been transported over long distances (Ding et al., 2013),
651 may instead have originated more locally from the western South Qinling Belt (Fig. 11).
652 Alternatively, these zircons could have been derived from previously deposited
653 (Paleozoic) sandstones within the basin, or from the inferred cratonic basement of the
654 South China Block even of the unexposed basement of the Songpan-Ganzi basin (e.g.,
655 Wang et al., 2016) (see Section 4.1).

656 For the Dabie Orogen to the east of the Qinling Orogenic Belt (Fig. 2), there is
657 limited evidence of magmatism during the Triassic and thus paleo-elevation estimates
658 are not available However, there are compositional similarities between the basement
659 of the Dabie Orogen and that of the South Qinling Belt (Wu and Zheng, 2013). It is
660 therefore plausible that the zircon in the Dabie Orogen originated from the South
661 Qinling Belt. In addition, there is no evidence of metamorphism (e.g., mica with high
662 Si content) in the sedimentary rocks of the Dabie Orogen (Enkelmann et al., 2007),
663 suggesting that this region was not a contributor to the Songpan-Ganzi basin. The
664 primary source of Paleoproterozoic to Archean-aged detrital zircons is believed to have
665 been the North China Block (Fig. 6), although it is possible that these zircons could
666 have originated in the North Qaidam region, with or without sediment recycling (Table
667 1) (Figs. 2, 10).

668 Igneous zircons derived from the East Kunlun region is prevalent in some samples
669 from the northeastern, central, and western depocenters (Table 1). This can be attributed
670 to ongoing surface uplift and rapid exhumation of the East Kunlun Orogen (Mock et

al., 1999; Jolivet et al., 2001; Liu et al., 2005; Dai et al., 2013). Our calculations suggest that the East Kunlun region may have reached a paleo-elevation of ca. 4000-5000 m. Paleocurrents measured in the East Kunlun region are consistently southwards (Liu et al., 2020 and references therein), which is consistent with a regional paleogeography in which Paleotethys lay to the south (Fig. 3).

The inferred, rapid exhumation rate during the Late Triassic (~0.8 km/Ma; Dai et al., 2013) and the estimated denudation thickness (0.4-1.2 km; Liu et al., 2020) of the East Kunlun region suggest that this region could also have contributed a significant amount of sediment into the Songpan-Ganzi basin to the south (Fig. 3).

The zircon grains that originated from the Qiangtang Block are likely to have been transported during the Middle Triassic, especially to the western, central, and southeastern depocenters (Table 1; Ding et al., 2013; Gong et al., 2021). As noted above, the lack of metamorphic detritus in the Songpan-Ganzi basin (Enkelmann et al., 2007) suggests that the ultra-high pressure metamorphic rocks of the Qiangtang region did not represent a significant source (cf. Zhang et al., 2008). Despite the relatively modest calculated paleo-elevation of North Qiangtang region (1000-3000 m) (see Section 5.5), this region contributed > 10% of detrital zircons (Table 1), mainly to the southeastern and western depocenters (Fig. 10), which is consistent with rapid erosion rate in the North Qiangtang Block.

Paleomagnetic data suggest that the North Qiangtang Block was situated within the range of ~25˚S to ~25˚N between 300 Ma and 200 Ma (Song et al., 2017, 2020). Regions that were located at relatively low latitudes could have experience intense tropical weathering (Deng et al., 2022; Zhang et al., 2022). This could help to explain why, despite its inferred relatively low elevation, the northern Qiangtang block contributed substantially to the zircons to the Songpan-Ganzi basin (Fig. 3).

As noted above, the Songpan-Ganzi basin was situated well below sea level until the Carnian (Fig. 10c) and was then uplifted to form a plateau-like feature (3000-4000 m) during the Norian to Rhaetian (Fig. 10d). Far-away sedimentary sources to the Songpan-Ganzi basin probably terminated before the Norian, although this is inconsistent with some previous interpretations (Weislogel et al., 2006, 2010; Enkelmann et al., 2007; Ding et al., 2013; Jian et al., 2019; Gong et al., 2021).

The zircon age populations from the Upper Triassic sandstones of the southwestern Sichuan Basin are distinct (Yan et al., 2019), as these formations (e.g., Xiaotangzi Formation) are characterized by a relatively high proportion of Paleozoic zircons compared to those of the underlying lithologies (e.g., Ma'antang Formation) (Yan et al., 2019). A similar pattern of Paleozoic zircons is commonly documented in the Songpan-Ganzi basin, suggesting that uplift of the basin was underway since the Norian, thereby making it possible to contribute sediment to the Sichuan Basin (Fig. 4).

In summary, the inferred sedimentary processes affecting the Triassic Songpan-Ganzi basin are consistent with the syn-collisional basin model, related to final closure of Paleotethys (e.g., Nie et al., 1994; Weislogel et al., 2006; Tang et al., 2023) (Fig. 3a). The sediments of the Songpan-Ganzi basin were contributed from multiple sources that were located in adjacent crustal units; this resulted in the observed local variations in sediment compositions within the different depocenters.

Our main conclusions are that: (1) the Qinling Orogenic Belt, despite its considerable calculated elevation, was only a minor contributor to the eastern depocenter; (2) input from the South China Block was minor, mainly restricted to the southeastern depocenter; (3) the East Kunlun Orogen, characterized by calculated high elevation, supplied all of the depocenters of the Songpan-Ganzi basin; (4) the North Qiangtang Block, despite its calculated lower elevation, represented the dominant

source of zircons found in the western, central and southeastern depocenters; (5) the Songpan-Ganzi basin underwent uplift during the Norian which triggered detrital supply to the Sichuan Basin.

It should, however, be emphasize that elevation may not have been the dominant control of the source contributions in all cases, as indicated by the above comparison of different sediment inputs from the North Qiangtang Block versus the Qinling Orogenic Belt. This supports some recent studies (Deng et al., 2022; Zhang et al., 2022) that have emphasized the importance of climate-related weathering in preference to e.g., tectonic uplift, relief and/or physical erosion processes. The results of our simulations (Fig. 9; Table 1) also suggest that zircon that were derived from different sources subsequently mixed within the basin, which may represent the effects of differential syn-collisional uplift.

This study has shown that by integrating statical analysis of detrital zircon age distributions with paleo-elevation calculations, it then became possible to estimate the contributions of sediment sources and also help to track the sediment pathways from source to sink. This combined approach has been shown to provide valuable insights to the complex sedimentary processes involved in the basin development within a complex region of on-going continental collision. We suggest that this combined approach should in future be applied to some other sedimentary basins of different ages; e.g., the Late Cretaceous-Eocene Mozambique Basin (Reading and Richards, 1994; Castelino et al., 2017), the Late Cretaceous-Miocene NW Sabah Basin (Malaysian Borneo) (van Hattum et al., 2006), or the modern easternmost Mediterranean Sea (Sagy et al., 2020).

## 7. Conclusions

The combination of detrital zircon geochronology through the application of source unmixing, and calculated paleo-elevations using empirical equations based on geochemical data from magmatic rocks, provide valuable insights into sedimentary source-to-sink relationships and the implications of changing paleo-altitudes in adjacent orogenic units.

For the Songpan-Ganzi basin sandstones specifically:

- Analysis of detrital zircon U-Pb age distributions, including both literature and original data (n=63), reveals the presence of five dominant populations: 300-200 Ma, 500-360 Ma, 1000-700 Ma, 2000-1600 Ma and 2600-2400 Ma.
- Multidimensional scaling and Monte Carlo Mixture modelling suggest a close relationship between the sandstones in the Songpan-Ganzi basin (sink) and the neighboring crustal units (proto-sources). Specifically, the North China Block (average contribution 12.3%), the North Qaidam Block (average contribution 14.8%), the East Kunlun magmatic rocks (average contribution 15.0%) and the Qiangtang magmatic rocks (average contribution 15.3%) are identified as the major zircon contributors for the Songpan-Ganzi basin .
- The input of detrital zircon from the Qinling Orogenic Belt, despite its calculated high elevation, was relatively minor and primarily restricted to the eastern part of the basin. Detrital zircons originating from the Qinling Orogenic Belt were mainly mixed with detritus derived from other sources and incorporated into the western depocenter during the Late Triassic, suggesting long-distance transport

767 and/or recycling from the eastern part of the basin during on-going continental
768 collision.

769 - Zircons derived from the South China Block primarily occur in the
770 southeastern depocenter and to a lesser extent in the western depocenter. This
771 distribution is consistent with the collision-related hypothesis of the Songpan-Ganzi
772 basin but does not conform to the expected age populations in the alternative back-
773 arc basin model.
774 - Zircons associated with the East Kunlun region were largely supplied to
775 the Songpan-Ganzi basin as a result of an inferred rise in paleo-elevation (4000-
776 5000 m), associated with rapid exhumation of the East Kunlun Orogen.
777 - The North Qiangtang Block, despite its inferred relatively low elevation,
778 contributed more than 10% of the detrital zircons to the four depocenters; this is
779 attributed to rapid erosion rate of this crustal block, possibly influenced by
780 climatically controlled weathering.

781 - The integrated method used in provenance analysis of Triassic sandstones
782 from the Songpan-Ganzi basin and the related magmatic rocks enables the
783 identification of different sources of detrital zircons. These sources were mainly the
784 adjacent crustal units. The resulting sediments mainly accumulated in four main
785 nearby depocenters within the Songpan-Ganzi basin. There is also some evidence
786 of sediment mixing and recycling within the basin during ongoing continental
787 collision.

788 - Basin-filling was primarily controlled by tectonically controlled surface
789 uplift combined with denudation of the adjacent mountain relevant belts, potentially

enhanced by climatically controlled weathering.

**Acknowledgments**

This study was funded by National Natural Science Foundation of China [grant numbers 42002126, 91755000, and 41902055]. The Yuneng Geological Service Corporation, Langfang assisted with the sample processing. Shitou Wu at the Institute of Geology and Geophysics, CAS is thanked for analytical assistance. We would like to the anonymous reviewer and the Editor Massimo Moretti for their constructive comments and suggestions.

**References**

Airy, G.B., 1855. On the computation of the effect of the attraction of mountain-masses, as disturbing the apparent astronomical latitude of stations in geodetic surveys. Philosophical Transactions of the Royal Society of London 145, 101-103.

Andersen, T., 2002. Correction of common lead in U–Pb analyses that do not report $^{204}$Pb. Chemical Geology 192, 59-79.

Andersen, T., 2005. Detrital zircons as tracers of sedimentary provenance: limiting conditions from statistics and numerical simulation. Chemical Geology 216, 249-270.

Andò, S., Morton, A., Garzanti, E., 2014. Metamorphic grade of source rocks revealed by chemical fingerprints of detrital amphibole and garnet, in: Scott, R.A., Smyth, H.R., Morton, A.C., Richardson, N. (Eds.), Sediment Provenance Studies in Hydrocarbon

812 Exploration and Production. Geological Society of London, Special Publications 386, 351-
813 371.
814 Belousova, E., Griffin, W., O'Reilly, S.Y., Fisher, N., 2002. Apatite as an indicator mineral for
815 mineral exploration: trace-element compositions and their relationship to host rock type.
816 Journal of Geochemical Exploration 76, 45-69.
817 Bruguier, O., Lancelot, J.R., Malavieille, J., 1997. U–Pb dating on single detrital zircon grains
818 from the Triassic Songpan–Ganze flysch (Central China): provenance and tectonic
819 correlations. Earth and Planetary Science Letters 152, 217-231.
820 Burchfiel, B.C., Zhiliang, C., Yupinc, L., Royden, L.H., 1995. Tectonics of the Longmen Shan
821 and adjacent regions, central China. International Geology Review 37, 661-735.
822 Castelino, J.A., Reichert, C., Jokat, W., 2017. Response of Cenozoic turbidite system to tectonic
823 activity and sea-level change off the Zambezi Delta. Marine Geophysical Research 38,
824 209-226.
825 Chaharlang, R., Ducea, M.N., Ghalamghash, J., 2020. Geochemical evidences for quantifying
826 crustal thickness over time in the Urumieh-Dokhtar magmatic arc (Iran). Lithos 374,
827 105723.
828 Chang, E.Z., 2000. Geology and tectonics of the Songpan-Ganzi fold belt, southwestern China.
829 International Geology Review 42, 813-831.
830 Chapman, J.B., Ducea, M.N., DeCelles, P.G., Profeta, L., 2015. Tracking changes in crustal
831 thickness during orogenic evolution with Sr/Y: An example from the North American
832 Cordillera. Geology 43, 919-922.
833 Chen, Y., Tang, J., Liu, F., Zhang, H.-f., Nie, L.-s., Jiang, L.-t., 2006. Elemental and Sm-Nd

isotopic geochemistry of clastic sedimentary rocks in the Garzê-Songpan block and Longmen Mountains (in Chinese with English abstract). Geology in China 33, 109-118.

Chen, Y., Zhang, G., Pei, X., Lu, R., Liang, W., Guo, X., 2010. Discussion on the formation age and tectonic implications of Dacaotan Group in West Qinling (in Chinese with English abstract). Acta Sedimentologica Sinica 28, 579-584.

Clift, P.D., Carter, A., Wysocka, A., Van Hoang, L., Zheng, H., Neubeck, N., 2020. A Late Eocene- Oligocene Through- Flowing River Between the Upper Yangtze and South China Sea. Geochemistry, Geophysics, Geosystems 21, e2020GC009046.

Dai, J., Wang, C., Hourigan, J., Santosh, M., 2013. Multi-stage tectono-magmatic events of the Eastern Kunlun Range, northern Tibet: insights from U–Pb geochronology and (U–Th)/He thermochronology. Tectonophysics 599, 97-106.

Darby, B.J., Gehrels, G., 2006. Detrital zircon reference for the North China block. Journal of Asian Earth Sciences 26, 637-648.

DeGraaff-Surpless, K., Mahoney, J.B., Wooden, J.L., McWilliams, M.O., 2003. Lithofacies control in detrital zircon provenance studies: Insights from the Cretaceous Methow basin, southern Canadian Cordillera. Geological Society of America Bulletin 115, 899-915.

Deng, K., Yang, S., Guo, Y., 2022. A global temperature control of silicate weathering intensity. Nature communications 13, 1781.

Dickinson, W.R., Gehrels, G.E., 2003. U–Pb ages of detrital zircons from Permian and Jurassic eolian sandstones of the Colorado Plateau, USA: paleogeographic implications. Sedimentary geology 163, 29-66.

Dickinson, W.R., Gehrels, G.E., 2008. Sediment delivery to the Cordilleran foreland basin:

856 Insights from U-Pb ages of detrital zircons in Upper Jurassic and Cretaceous strata of the
857 Colorado Plateau. American Journal of Science 308, 1041-1082.
858 Ding, L., Yang, D., Cai, F.L., Pullen, A., Kapp, P., Gehrels, G.E., Zhang, L.Y., Zhang, Q.H.,
859 Lai, Q.Z., Yue, Y.H., 2013. Provenance analysis of the Mesozoic Hoh- Xil- Songpan-
860 Ganzi turbidites in northern Tibet: Implications for the tectonic evolution of the eastern
861 Paleo- Tethys Ocean. Tectonics 32, 34-48.
862 Diwu, C., Sun, Y., Liu, L., Zhang, C., Wang, H., 2010. The disintegration of Kuanping Group
863 in North Qinling orogenic belts and Neo-proterozoic N-MORB (in Chinese with English
864 abstract). Acta Petrologica Sinica 26, 2025-2038.
865 Diwu, C., Sun, Y., Zhao, Y., Liu, B., Lai, S., 2014. Geochronological, geochemical, and Nd-Hf
866 isotopic studies of the Qinling Complex, central China: Implications for the evolutionary
867 history of the North Qinling Orogenic Belt. Geoscience Frontiers 5, 499-513.
868 Dodson, M., Compston, W., Williams, I., Wilson, J., 1988. A search for ancient detrital zircons
869 in Zimbabwean sediments. Journal of the Geological Society 145, 977-983.
870 Dong, Y., He, D., Sun, S., Liu, X., Zhou, X., Zhang, F., Yang, Z., Cheng, B., Zhao, G., Li, J.,
871 2018. Subduction and accretionary tectonics of the East Kunlun orogen, western segment
872 of the Central China Orogenic System. Earth-Science Reviews 186, 231-261.
873 Dong, Y., Liu, X., Neubauer, F., Zhang, G., Tao, N., Zhang, Y., Zhang, X., Li, W., 2013. Timing
874 of Paleozoic amalgamation between the North China and South China Blocks: evidence
875 from detrital zircon U–Pb ages. Tectonophysics 586, 173-191.
876 Dong, Y., Santosh, M., 2016. Tectonic architecture and multiple orogeny of the Qinling
877 Orogenic Belt, Central China. Gondwana Research 29, 1-40.

878 Duan, L., 2010. Detrital zircon provenance of the Silurian and Devonian in South Qinling, and
879 the northwestern margin of Yangtze terrane and its tectonic implications. Northwest
880 University, Xi'an, China, pp. 1-83.
881 Enkelmann, E., Weislogel, A., Ratschbacher, L., Eide, E., Renno, A., Wooden, J., 2007. How
882 was the Triassic Songpan-Ganzi basin filled? A provenance study. Tectonics 26.
883 Faure, M., Lin, W., Le Breton, N., 2001. Where is the North China–South China block boundary
884 in eastern China? Geology 29, 119-122.
885 Fedo, C.M., Sircombe, K.N., Rainbird, R.H., 2003. Detrital zircon analysis of the sedimentary
886 record. Reviews in mineralogy and geochemistry 53, 277-303.
887 Garzanti, E., Andò, S., 2019. Heavy minerals for junior woodchucks. Minerals 9, 148.
888 Garzanti, E., Vermeesch, P., Andò, S., Vezzoli, G., Valagussa, M., Allen, K., Kadi, K.A., Al-
889 Juboury, A.I., 2013. Provenance and recycling of Arabian desert sand. Earth-Science
890 Reviews 120, 1-19.
891 Gehrels, G., 2011. Detrital zircon U- Pb geochronology: Current methods and new
892 opportunities, in: Busby, C., Azor, A. (Eds.), Tectonics of sedimentary basins: Recent
893 advances. John Wiley & Sons, Chichester, pp. 47-62.
894 Gehrels, G.E., 2000. Introduction to detrital zircon studies of Paleozoic and Triassic strata in
895 western Nevada and northern California, in: Soreghan, M., Gehrels, G. (Eds.), Paleozoic
896 and Triassic Paleogeography and Tectonics of Western Nevada and Northern California.
897 Geological Society of America, Special Papers 347, pp. 1-18.
898 Gehrels, G., Kapp, P., DeCelles, P., Pullen, A., Blakey, R., Weislogel, A., Ding, L., Guynn, J.,
899 Martin, A., McQuarrie, N., Yin, A. 2011. Detrital zircon geochronology of pre- Tertiary

900 strata in the Tibetan- Himalayan orogen. Tectonics 30, TC5016.
901 Gehrels, G.E., Valencia, V.A., Ruiz, J., 2008. Enhanced precision, accuracy, efficiency, and
902 spatial resolution of U- Pb ages by laser ablation–multicollector–inductively coupled
903 plasma–mass spectrometry. Geochemistry, Geophysics, Geosystems 9, Q03017.
904 Gong, D.-X., Wu, C.-H., Zou, H., Zhou, X., Zhou, Y., Tan, H.-Q., Yue, X.-Y., 2021. Provenance
905 analysis of Late Triassic turbidites in the eastern Songpan–Ganzi Flysch Complex:
906 Sedimentary record of tectonic evolution of the eastern Paleo-Tethys Ocean. Marine and
907 Petroleum Geology 126, 104927.
908 Griffin, W., 2008. GLITTER: Data reduction software for laser ablation ICP-MS, in: Sylvester,
909 P. (Ed.), Laser Ablation ICP-MS in the Earth Sciences: Current practices and outstanding
910 issues. Mineralogical Association of Canada: Short Course Series 40, pp. 307-311.
911 Grigsby, J.D., 1990. Detrital magnetite as a provenance indicator. Journal of Sedimentary
912 Research 60, 940-951.
913 Gu, X., 1994. Geochemical characteristics of the Triassic Tethys-turbidites in northwestern
914 Sichuan, China: implications for provenance and interpretation of the tectonic setting.
915 Geochimica et Cosmochimica Acta 58, 4615-4631.
916 He, J., Garzanti, E., Cao, L., Wang, H., 2020. The zircon story of the Pearl River (China) from
917 Cretaceous to present. Earth-Science Reviews 201, 103078.
918 He, S., Li, R., Wang, C., Zhang, H., Ji, W., Yu, P., Gu, P., Shi, C. 2011. Discovery of∼ 4.0 Ga
919 detrital zircons in the Changdu Block, North Qiangtang, Tibetan Plateau. Chinese Science
920 Bulletin 56, 647-658.
921 Hillenbrand, I.W., Williams, M.L., 2021. Paleozoic evolution of crustal thickness and elevation

in the northern Appalachian orogen, USA. Geology 49, 946-951.

Hu, F., Ducea, M.N., Liu, S., Chapman, J.B., 2017. Quantifying crustal thickness in continental collisional belts: Global perspective and a geologic application. Scientific reports 7, 7058.

Hu, F., Liu, S., Ducea, M.N., Chapman, J.B., Wu, F., Kusky, T., 2020a. Early Mesozoic magmatism and tectonic evolution of the Qinling Orogen: Implications for oblique continental collision. Gondwana Research 88, 296-332.

Hu, F., Wu, F., Chapman, J.B., Ducea, M.N., Ji, W., Liu, S., 2020b. Quantitatively tracking the elevation of the Tibetan Plateau since the cretaceous: Insights from whole- rock Sr/Y and La/Yb ratios. Geophysical Research Letters 47, e2020GL089202.

Hu, F., Wu, F.Y., Chen, G.H., Yang, L., 2022. The critical factors of lithium enrichment in the metasedimentary wall rocks of granitic pegmatite-type lithium deposit: Insights from the Ke'eryin area in the eastern Songpan-Ganzi Belt. Acta Petrologica Sinica 38, 2017-2051.

Huang, C., Wang, H., Yang, J.H., Ramezani, J., Yang, C., Zhang, S.B., Yang, Y.H., Xia, X.P., Feng, L.J., Lin, J., 2020. SA01–A Proposed Zircon Reference Material for Microbeam U-Pb Age and Hf- O Isotopic Determination. Geostandards and Geoanalytical Research 44, 103-123.

Huang, X., Zhang, H., Wang, X., Wang, X., Wang, Z., Qi, Y., 2017. LA-ICP-MS U-Pb dating of detrital zircons from the Upper Permian Gequ Formation on the southern margin of the East Kunlun Mountains and its tectonics implications (in Chinese with English abstract). Geological Bulletin of China 36, 258-269.

Jian, X., Weislogel, A., Pullen, A., 2019. Triassic sedimentary filling and closure of the eastern Paleo- Tethys Ocean: New insights from detrital zircon geochronology of Songpan-

944 Ganzi, Yidun, and West Qinling flysch in eastern Tibet. Tectonics 38, 767-787.
945 Jolivet, M., Brunel, M., Seward, D., Xu, Z., Yang, J., Roger, F., Tapponnier, P., Malavieille, J.,
946 Arnaud, N., Wu, C., 2001. Mesozoic and Cenozoic tectonics of the northern edge of the
947 Tibetan plateau: fission-track constraints. Tectonophysics 343, 111-134.
948 Kapp, P., DeCelles, P.G., 2019. Mesozoic–Cenozoic geological evolution of the Himalayan-
949 Tibetan orogen and working tectonic hypotheses. American Journal of Science 319, 159-
950 254.
951 Kapp, P., Yin, A., Manning, C.E., Harrison, T.M., Taylor, M.H., Ding, L., 2003. Tectonic
952 evolution of the early Mesozoic blueschist- bearing Qiangtang metamorphic belt, central
953 Tibet. Tectonics 22, 1043.
954 Kapp, P., Yin, A., Manning, C.E., Murphy, M., Harrison, T.M., Spurlin, M., Lin, D., Xi-Guang,
955 D., Cun-Ming, W., 2000. Blueschist-bearing metamorphic core complexes in the
956 Qiangtang block reveal deep crustal structure of northern Tibet. Geology 28, 19-22.
957 Kirby, E., Reiners, P.W., Krol, M.A., Whipple, K.X., Hodges, K.V., Farley, K.A., Tang, W.,
958 Chen, Z., 2002. Late Cenozoic evolution of the eastern margin of the Tibetan Plateau:
959 Inferences from $^{40}Ar/^{39}Ar$ and (U- Th)/He thermochronology. Tectonics 21, 1001.
960 Kröner, A., Compston, W., Guo-Wei, Z., An-Lin, G., Todt, W., 1988. Age and tectonic setting
961 of Late Archean greenstone-gneiss terrain in Henan Province, China, as revealed by
962 single-grain zircon dating. Geology 16, 211-215.
963 Lee, C.-T.A., Thurner, S., Paterson, S., Cao, W., 2015. The rise and fall of continental arcs:
964 Interplays between magmatism, uplift, weathering, and climate. Earth and Planetary
965 Science Letters 425, 105-119.

León, S., Monsalve, G., Bustamante, C., 2021. How much did the Colombian Andes rise by the collision of the Caribbean oceanic plateau? Geophysical Research Letters 48, e2021GL093362.

Li, Q., Liu, S., Wang, Z., Chu, Z., Song, B., Wang, Y., Wang, T., 2008. Contrasting provenance of Late Archean metasedimentary rocks from the Wutai Complex, North China Craton: detrital zircon U–Pb, whole-rock Sm–Nd isotopic, and geochemical data. International Journal of Earth Sciences 97, 443-458.

Li, S., Zhao, S., Liu, X., Cao, H., Yu, S., Li, X., Somerville, I., Yu, S., Suo, Y., 2018. Closure of the Proto-Tethys Ocean and Early Paleozoic amalgamation of microcontinental blocks in East Asia. Earth-Science Reviews 186, 37-75.

Ling, W., Duan, R., Liu, X., Cheng, J., Mao, X., Peng, L., Liu, Z., Yang, H., Ren, B., 2010. U-Pb dating of detrital zircons from the Wudangshan Group in the South Qinling and its geological significance. Chinese Science Bulletin 55, 2440-2448.

Lipman, P.W., 2021. Raising the West: Mid-Cenozoic Colorado-plano related to subvolcanic batholith assembly in the Southern Rocky Mountains (USA)? Geology 49, 1107-1111.

Liu, C., Zhao, G., Sun, M., Zhang, J., He, Y., Yin, C., Wu, F., Yang, J., 2011. U-Pb and Hf isotopic study of detrital zircons from the Hutuo group in the Trans-North China Orogen and tectonic implications. Gondwana Research 20, 106-121.

Liu, K., Li, Z., Shi, X., Wei, X., Ren, Z., Yang, X., Peng, B., 2020. Late Hercynian-Indosinian denudation and uplift history in the eastern Qaidam Basin: constraints from multiple thermometric indicators and sedimentary evidences. Chinese Journal of Geophysics 63, 1403-1421 (in Chinese with English abstract).

988 Liu, X., Gao, S., Diwu, C., Ling, W., 2008. Precambrian crustal growth of Yangtze Craton as
989 revealed by detrital zircon studies. American Journal of Science 308, 421-468.
990 Liu, Y., Genser, J., Neubauer, F., Jin, W., Ge, X., Handler, R., Takasu, A., 2005. $^{40}Ar/^{39}Ar$
991 mineral ages from basement rocks in the Eastern Kunlun Mountains, NW China, and their
992 tectonic implications. Tectonophysics 398, 199-224.
993 Lu, L., Qin, Y., Li, Z.-F., Yan, L.-L., Jin, X., Zhang, K.-J., 2019. Diachronous closure of the
994 Shuanghu Paleo-Tethys Ocean: constraints from the Late Triassic Tanggula arc-related
995 volcanism in the East Qiangtang subterrane, Central Tibet. Lithos 328, 182-199.
996 Ludwig, K.R., 2008. User's Manual for Isoplot 3.6: A Geochronological Toolkit for Microsoft
997 Excel. Berkeley Geochronology Center Special Publication, Berkeley.
998 Luffi, P., Ducea, M., 2022. Chemical mohometry: Assessing crustal thickness of ancient
999 orogens using geochemical and isotopic data. Reviews of Geophysics 60,
1000 e2021RG000753.
1001 Malusà, M.G., Garzanti, E., 2019. The sedimentology of detrital thermochronology, in: Malusà,
1002 M.G., Fitzgerald, P.G. (Eds.), Fission-track Thermochronology and its Application to
1003 Geology. Springer, Cham, Switzerland, pp. 123-143.
1004 Mange, M.A., Maurer, H., 1991. Heavy Minerals in Colour. Chapman and Hall, London.
1005 McDonough, W.F., Sun, S.-s., 1995. The composition of the Earth. Chemical Geology 120,
1006 223-253.
1007 McLennan, S., Bock, B., Compston, W., Hemming, S., McDaniel, D., 2001. Detrital zircon
1008 geochronology of Taconian and Acadian foreland sedimentary rocks in New England.
1009 Journal of Sedimentary Research 71, 305-317.

1010 Meinhold, G., 2010. Rutile and its applications in earth sciences. Earth-Science Reviews 102,
1011 1-28.
1012 Meng, Q.-R., Wu, G.-L., Fan, L.-G., Wei, H.-H., 2019. Tectonic evolution of early Mesozoic
1013 sedimentary basins in the North China block. Earth-Science Reviews 190, 416-438.
1014 Mock, C., Arnaud, N.O., Cantagrel, J.-M., 1999. An early unroofing in northeastern Tibet?
1015 Constraints from $^{40}Ar/^{39}Ar$ thermochronology on granitoids from the eastern Kunlun range
1016 (Qianghai, NW China). Earth and Planetary Science Letters 171, 107-122.
1017 Moghadam, H.S., Li, Q.-L., Griffin, W.L., Stern, R.J., Santos, J.F., Ducea, M.N., Ottley, C.J.,
1018 Karsli, O., Sepidbar, F., O'Reilly, S.Y., 2022. Temporal changes in subduction-to collision-
1019 related magmatism in the Neotethyan orogen: the Southeast Iran example. Earth-Science
1020 Reviews 226, 103930.
1021 Morton, A.C., 1991. Geochemical studies of detrital heavy minerals and their application to
1022 provenance research, in: Morton, A.C., Todd, S.P., Haughton, P.D.W. (Eds.),
1023 Developments in Sedimentary Provenance Studies. Geological Society of London, Special
1024 Publications 57, pp. 31-45.
1025 Morton, A.C., Hallsworth, C., 1994. Identifying provenance-specific features of detrital heavy
1026 mineral assemblages in sandstones. Sedimentary geology 90, 241-256.
1027 Nie, S., Yin, A., Rowley, D.B., Jin, Y., 1994. Exhumation of the Dabie Shan ultra-high-pressure
1028 rocks and accumulation of the Songpan-Ganzi flysch sequence, central China. Geology
1029 22, 999-1002.
1030 Pan, G.-t., Ding, J., Yao, D.-s., Wang, L.-q., 2004. Geological Map of the Qinghai-Xizang (Tibet)
1031 Plateau and Adjacent Areas with Guidebook. Chengdu Cartographic Publishing House,

scale 1:1500000, Chengdu, China.

Pan, Y., Hu, X. A database of detrital zircon U–Pb geochronology and Hf isotopes from the Songpan–Ganzi and Western Qinling terranes. Geoscience Data Journal, 1-11.

Profeta, L., Ducea, M.N., Chapman, J.B., Paterson, S.R., Gonzales, S.M.H., Kirsch, M., Petrescu, L., DeCelles, P.G., 2015. Quantifying crustal thickness over time in magmatic arcs. Scientific reports 5, 1-7.

Province, B.o.G.a.M.R.o.S., 1991. Regional Geology of Sichuan Province. Geological Publishing House, Beijing.

Pullen, A., Kapp, P., Gehrels, G.E., Vervoort, J.D., Ding, L., 2008. Triassic continental subduction in central Tibet and Mediterranean-style closure of the Paleo-Tethys Ocean. Geology 36, 351-354.

Reading, H.G., Richards, M., 1994. Turbidite systems in deep-water basin margins classified by grain size and feeder system. AAPG bulletin 78, 792-822.

Reid, A., Wilson, C. J., Shun, L., Pearson, N., Belousova, E. 2007. Mesozoic plutons of the Yidun Arc, SW China: U/Pb geochronology and Hf isotopic signature. Ore Geology Reviews 31, 88-106.

Roger, F., Arnaud, N., Gilder, S., Tapponnier, P., Jolivet, M., Brunel, M., Malavieille, J., Xu, Z., Yang, J., 2003. Geochronological and geochemical constraints on Mesozoic suturing in east central Tibet. Tectonics 22.

Roger, F., Jolivet, M., Cattin, R., Malavieille, J., 2011. Mesozoic-Cenozoic tectonothermal evolution of the eastern part of the Tibetan Plateau (Songpan-Garzê, Longmen Shan area): insights from thermochronological data and simple thermal modelling, in: Gloaguen, R.,

Ratschbacher, L. (Eds.), Growth and Collapse of the Tibetan Plateau. Geological Society, London, Special Publications 353, pp. 9-25.

Rubatto, D., 2002. Zircon trace element geochemistry: partitioning with garnet and the link between U–Pb ages and metamorphism. Chemical Geology 184, 123-138.

Sagy, Y., Dror, O., Gardosh, M., Reshef, M., 2020. The origin of the Pliocene to recent succession in the Levant basin and its depositional pattern, new insight on source to sink system. Marine and Petroleum Geology 120, 104540.

Saylor, J.E., Sundell, K.E., 2016. Quantifying comparison of large detrital geochronology data sets. Geosphere 12, 203-220.

She, Z., Ma, C., Mason, R., Li, J., Wang, G., Lei, Y., 2006. Provenance of the Triassic Songpan–Ganzi flysch, west China. Chemical Geology 231, 159-175.

Shi, Y., Yu, J.-H., Santosh, M., 2013. Tectonic evolution of the Qinling orogenic belt, Central China: new evidence from geochemical, zircon U–Pb geochronology and Hf isotopes. Precambrian Research 231, 19-60.

Sircombe, K., Hazelton, M., 2004. Comparison of detrital zircon age distributions by kernel functional estimation. Sedimentary geology 171, 91-111.

Sircombe, K.N., 2004. AgeDisplay: an EXCEL workbook to evaluate and display univariate geochronological data using binned frequency histograms and probability density distributions. Computers & Geosciences 30, 21-31.

Smyth, H.R., Morton, A., Richardson, N., Scott, R.A., 2014. Sediment provenance studies in hydrocarbon exploration and production: An introduction, in: Scott, R.A., Smyth, H.R., Morton, A.C., Richardson, N. (Eds.), Sediment Provenance Studies in Hydrocarbon

Exploration and Production. Geological Society of London, Special Publications 386, pp. 1-6.

Song, P., Ding, L., Li, Z., Lippert, P.C., Yue, Y., 2017. An early bird from Gondwana: Paleomagnetism of Lower Permian lavas from northern Qiangtang (Tibet) and the geography of the Paleo-Tethys. Earth and Planetary Science Letters 475, 119-133.

Song, P., Ding, L., Lippert, P.C., Li, Z., Zhang, L., Xie, J., 2020. Paleomagnetism of Middle Triassic lavas from northern Qiangtang (Tibet): Constraints on the closure of the Paleo-Tethys Ocean. Journal of Geophysical Research: Solid Earth 125, e2019JB017804.

Su, B., Chen, Y., Liu, F., Wang, Q., Zhang, H., Lan, Z., 2006. Geochemical characteristics and significance of Triassic sandstones of Songpan-Ganze block (in Chinese with English abstract). Acta Petrologica Sinica 22, 961-970.

Sun, J., Dong, Y., Ma, L., Chen, S., Jiang, W., 2022. Devonian to Triassic tectonic evolution and basin transition in the East Kunlun–Qaidam area, northern Tibetan Plateau: Constraints from stratigraphy and detrital zircon U–Pb geochronology. GSA Bulletin 134, 1967-1993.

Sun, J., Dong, Y., Ma, L., Peng, Y., Chen, S., Du, J., Jiang, W., 2019. Late Paleoproterozoic tectonic evolution of the Olongbuluke Terrane, northern Qaidam, China: Constraints from stratigraphy and detrital zircon geochronology. Precambrian Research 331, 105349.

Sun, W.-H., Zhou, M.-F., Gao, J.-F., Yang, Y.-H., Zhao, X.-F., Zhao, J.-H., 2009. Detrital zircon U–Pb geochronological and Lu–Hf isotopic constraints on the Precambrian magmatic and crustal evolution of the western Yangtze Block, SW China. Precambrian Research 172, 99-126.

1098 Sun, W.-H., Zhou, M.-F., Yan, D.-P., Li, J.-W., Ma, Y.-X., 2008. Provenance and tectonic setting
1099 of the Neoproterozoic Yanbian Group, western Yangtze block (SW China). Precambrian
1100 Research 167, 213-236.
1101 Sundell, K.E., Laskowski, A.K., Kapp, P., Ducea, M., Chapman, J., 2021. Jurassic to Neogene
1102 quantitative crustal thickness estimates in southern Tibet. GSA today 31, 4-10.
1103 Sundell, K.E., Saylor, J.E., 2017. Unmixing detrital geochronology age distributions.
1104 Geochemistry, Geophysics, Geosystems 18, 2872-2886.
1105 Tang, M., Ji, W.-Q., Chu, X., Wu, A., Chen, C., 2021. Reconstructing crustal thickness
1106 evolution from europium anomalies in detrital zircons. Geology 49, 76-80.
1107 Tang, Y., Yin, A., Xu, X., An, K., Zhang, Y., 2023. Tectonic evolution of the Triassic Songpan-
1108 Ganzi basin as constrained by a synthesis of multi- proxy provenance data. Basin
1109 Research 35, 28-60.
1110 Tang, Y., Zhang, Y., Tong, L., 2018. Mesozoic-Cenozoic evolution of the Zoige depression in
1111 the Songpan-Ganzi flysch basin, eastern Tibetan Plateau: Constraints from detrital zircon
1112 U-Pb ages and fission-track ages of the Triassic sedimentary sequence. Journal of Asian
1113 Earth Sciences 151, 285-300.
1114 Tian, Z. D., Leng, C. B., Zhang, X. C. 2020. Provenance and tectonic setting of the
1115 Neoproterozoic meta-sedimentary rocks at southeastern Tibetan Plateau: Implications for
1116 the tectonic affinity of Yidun terrane. Precambrian Research 344, 105736.
1117 Tung, K., Yang, H.-J., Yang, H.-Y., Liu, D., Zhang, J., Wan, Y., Tseng, C.-Y., 2007. SHRIMP
1118 U-Pb geochronology of the zircons from the Precambrian basement of the Qilian Block
1119 and its geological significances. Chinese Science Bulletin 52, 2687-2701.

van Hattum, M.W., Hall, R., Pickard, A.L., Nichols, G.J., 2006. Southeast Asian sediments not from Asia: Provenance and geochronology of north Borneo sandstones. Geology 34, 589-592.

Vermeesch, P., 2004. How many grains are needed for a provenance study? Earth and Planetary Science Letters 224, 441-451.

Vermeesch, P., 2012. On the visualisation of detrital age distributions. Chemical Geology 312, 190-194.

Vermeesch, P., 2013. Multi-sample comparison of detrital age distributions. Chemical Geology 341, 140-146.

Vermeesch, P., Garzanti, E., 2015. Making geological sense of 'Big Data' in sedimentary provenance analysis. Chemical Geology 409, 20-27.

Vermeesch, P., Resentini, A., Garzanti, E., 2016. An R package for statistical provenance analysis. Sedimentary geology 336, 14-25.

von Eynatten, H., Gaupp, R., 1999. Provenance of Cretaceous synorogenic sandstones in the Eastern Alps: constraints from framework petrography, heavy mineral analysis and mineral chemistry. Sedimentary geology 124, 81-111.

Wan, Y., Liu, D., Dong, C., Yin, X., 2011a. SHRIMP zircon dating of meta-sedimentary rock from the Qinling Group in the north of Xixia, North Qinling Orogenic Belt: constraints on complex histories of source region and timing of deposition and metamorphism (in Chinese with English abstract). Acta Petrologica Sinica 27, 1172-1178.

Wan, Y., Liu, D., Wang, W., Song, T., Kröner, A., Dong, C., Zhou, H., Yin, X., 2011b. Provenance of Meso-to Neoproterozoic cover sediments at the Ming Tombs, Beijing,

North China Craton: an integrated study of U–Pb dating and Hf isotopic measurement of detrital zircons and whole-rock geochemistry. Gondwana Research 20, 219-242.

Wang, H., Gao, R., Zhang, J., Li, Q., Guan, Y., Li, W., Guo, X., Li, H., 2016. Research of the crustal property of the Songpan-Garze block. Chinese Journal of Geology 51, 41-52.

Wang, J., Fu, X., Wei, H., Shen, L., Wang, Z., Li, K., 2022. Late Triassic basin inversion of the Qiangtang Basin in northern Tibet: Implications for the closure of the Paleo-Tethys and expansion of the Neo-Tethys. Journal of Asian Earth Sciences 227, 105119.

Wang, J., Li, Z. X., 2003. History of Neoproterozoic rift basins in South China: implications for Rodinia break-up. Precambrian Research 122, 141-158.

Wang, L.-J., Griffin, W., Yu, J.-H., O'Reilly, S., 2013. U–Pb and Lu–Hf isotopes in detrital zircon from Neoproterozoic sedimentary rocks in the northern Yangtze Block: implications for Precambrian crustal evolution. Gondwana Research 23, 1261-1272.

Wang, L.-J., Griffin, W.L., Yu, J.-H., O'Reilly, S.Y., 2010. Precambrian crustal evolution of the Yangtze Block tracked by detrital zircons from Neoproterozoic sedimentary rocks. Precambrian Research 177, 131-144.

Wang, L.-J., Yu, J.-H., Griffin, W., O'Reilly, S., 2012. Early crustal evolution in the western Yangtze Block: evidence from U–Pb and Lu–Hf isotopes on detrital zircons from sedimentary rocks. Precambrian Research 222, 368-385.

Wang, L., Pan, G., 2013. 1:1.5 million geological map of Tibetan Plateau and its surrounding areas. Geological Press, Beijing.

Wang, W., Cawood, P. A., Liu, S., Guo, R., Bai, X., Wang, K. 2017. Cyclic formation and stabilization of Archean lithosphere by accretionary orogenesis: Constraints from TTG

and potassic granitoids, North China Craton. Tectonics 36, 1724-1742.

Wang, Y., Pei, X., Liu, C., Li, R., Li, Z., Wei, B., Ren, H., Chen, W., Liu, T., Xu, X., 2014. Detrial zircon LA-ICP-MS U–Pb ages of the Devonian Shujiaba Group in Shujiaba area of the West Qinling tectonic zone: constraints on material source and sedimentary age (in Chinese with English abstract). Geological Bulletin of China 33, 1015-1027.

Weislogel, A.L., 2008. Tectonostratigraphic and geochronologic constraints on evolution of the northeast Paleotethys from the Songpan-Ganzi complex, central China. Tectonophysics 451, 331-345.

Weislogel, A.L., Graham, S.A., Chang, E.Z., Wooden, J.L., Gehrels, G.E., 2010. Detrital zircon provenance from three turbidite depocenters of the Middle–Upper Triassic Songpan-Ganzi complex, central China: Record of collisional tectonics, erosional exhumation, and sediment production. Geological Society of America Bulletin 122, 2041-2062.

Weislogel, A.L., Graham, S.A., Chang, E.Z., Wooden, J.L., Gehrels, G.E., Yang, H., 2006. Detrital zircon provenance of the Late Triassic Songpan-Ganzi complex: Sedimentary record of collision of the North and South China blocks. Geology 34, 97-100.

Wiedenbeck, M., Alle, P., Corfu, F.y., Griffin, W., Meier, M., Oberli, F.v., Quadt, A.v., Roddick, J., Spiegel, W., 1995. Three natural zircon standards for U- Th- Pb, Lu- Hf, trace element and REE analyses. Geostandards newsletter 19, 1-23.

Wu, C., Zuza, A.V., Chen, X., Ding, L., Levy, D.A., Liu, C., Liu, W., Jiang, T., Stockli, D.F., 2019. Tectonics of the Eastern Kunlun Range: Cenozoic reactivation of a Paleozoic- early Mesozoic orogen. Tectonics 38, 1609-1650.

Wu, F.-Y., Wan, B., Zhao, L., Xiao, W., Zhu, R., 2020. Tethyan geodynamics. Acta Petrologica

1186 Sinica 36, 1627-1674 (in Chinese with English abstract).
1187 Wu, S., Pei, X., Li, Z., Li, R., Pei, L., Chen, Y., Gao, J., Liu, C., Wei, F., Wang, Y., 2012. A
1188 study of the material source of Dacaotan Group in the northern margin of West Qinling
1189 orogenic belt: LA-ICP-MS U-Th-Pb age evidence of detrital zircons (in Chinese with
1190 English abstract). Geological Bulletin of China 31, 1470-1480.
1191 Wu, Y.-B., Zheng, Y.-F., 2013. Tectonic evolution of a composite collision orogen: an overview
1192 on the Qinling–Tongbai–Hong'an–Dabie–Sulu orogenic belt in central China. Gondwana
1193 Research 23, 1402-1428.
1194 Xia, X., Sun, M., Zhao, G., Luo, Y., 2006a. LA-ICP-MS U–Pb geochronology of detrital zircons
1195 from the Jining Complex, North China Craton and its tectonic significance. Precambrian
1196 Research 144, 199-212.
1197 Xia, X., Sun, M., Zhao, G., Wu, F., Xu, P., Zhang, J., Luo, Y., 2006b. U–Pb and Hf isotopic
1198 study of detrital zircons from the Wulashan khondalites: constraints on the evolution of
1199 the Ordos Terrane, Western Block of the North China Craton. Earth and Planetary Science
1200 Letters 241, 581-593.
1201 Xie, L., Zhang, Y., Zhang, H., Sun, J., Wu, F., 2008. In situ simultaneous determination of trace
1202 elements, U-Pb and Lu-Hf isotopes in zircon and baddeleyite. Chinese Science Bulletin
1203 53, 1565-1573.
1204 Yan, Z., Aitchison, J.C., Fu, C., Guo, X., Xia, W., Niu, M., 2016a. Devonian sedimentation in
1205 the Xiqingshan Mountains: Implications for paleogeographic reconstructions of the SW
1206 Qinling Orogen. Sedimentary geology 343, 1-17.
1207 Yan, Z., Fu, C., Wang, Z., Yan, Q., Chen, L., Chen, J., 2016b. Late Paleozoic subduction–

accretion along the southern margin of the North Qinling terrane, central China: evidence from zircon U-Pb dating and geochemistry of the Wuguan Complex. Gondwana Research 30, 97-111.

Yan, Z., Tian, Y., Li, R., Vermeesch, P., Sun, X., Li, Y., Rittner, M., Carter, A., Shao, C., Huang, H., 2019. Late Triassic tectonic inversion in the upper Yangtze Block: Insights from detrital zircon U–Pb geochronology from south- western Sichuan Basin. Basin Research 31, 92-113.

Yang, W., Peng, S., Wang, M., Zhang, H., 2021. Provenance of upper Permian–Triassic sediments in the south of North China: Implications for the Qinling orogeny and basin evolution. Sedimentary geology 424, 106002.

Yin, A., Nie, S., 1993. An indentation model for the North and South China collision and the development of the Tan- Lu and Honam fault systems, eastern Asia. Tectonics 12, 801-813.

Yu, M., Dick, J., Feng, C., Li, B., Wang, H., 2020. The tectonic evolution of the East Kunlun Orogen, northern Tibetan Plateau: A critical review with an integrated geodynamic model. Journal of Asian Earth Sciences 191, 104168.

Zhai, M., 2010. Tectonic evolution and metallogenesis of North China Craton. Mineral Deposits 29, 24-36 (in Chinese with English abstract)

Zhan, Q.Y., Zhu, D.C., Wang, Q., Cawood, P.A., Xie, J.C., Li, S.M., Wang, R., Zhang, L.L., Zhao, Z.D., Deng, J., 2018. Constructing the eastern margin of the Tibetan Plateau during the Late Triassic. Journal of Geophysical Research: Solid Earth 123, 10449-10459.

Zhang, C., 2019. Triassic Sedimentary Filling and Tectonic Evolution in Bayan Har Basin.

Northwest University, Xi'an, China, pp. 1-228.

Zhang, F., Dellinger, M., Hilton, R.G., Yu, J., Allen, M.B., Densmore, A.L., Sun, H., Jin, Z., 2022. Hydrological control of river and seawater lithium isotopes. Nature communications 13, 3359.

Zhang, K.-J., Li, B., Wei, Q.-G., 2012. Diversified provenance of the Songpan-Ganzi Triassic turbidites, central China: constraints from geochemistry and Nd isotopes. The Journal of Geology 120, 69-82.

Zhang, K.-J., Li, B., Wei, Q.-G., Cai, J.-X., Zhang, Y.-X., 2008. Proximal provenance of the western Songpan–Ganzi turbidite complex (Late Triassic, eastern Tibetan plateau): Implications for the tectonic amalgamation of China. Sedimentary geology 208, 36-44.

Zhang, Y.-X., Tang, X.-C., Zhang, K.-J., Zeng, L., Gao, C.-L., 2014. U–Pb and Lu–Hf isotope systematics of detrital zircons from the Songpan–Ganzi Triassic flysch, NE Tibetan Plateau: Implications for provenance and crustal growth. International Geology Review 56, 29-56.

Zhang, Z., Li, S., Cao, H., Somerville, I., Zhao, S., Yu, S., 2015. Origin of the North Qinling microcontinent and Proterozoic geotectonic evolution of the Kuanping Ocean, Central China. Precambrian Research 266, 179-193.

Zhao, G., Sun, M., Wilde, S. A., Sanzhong, L., 2005. Late Archean to Paleoproterozoic evolution of the North China Craton: key issues revisited. Precambrian Research 136, 177-202.

Zhao, J. H., Zhou, M. F., Yan, D. P., Zheng, J. P., Li, J. W., 2011. Reappraisal of the ages of Neoproterozoic strata in South China: no connection with the Grenvillian orogeny.

Geology 39, 299-302

Zhao, S., Li, S., Liu, X., Santosh, M., Somerville, I., Cao, H., Yu, S., Zhang, Z., Guo, L., 2015. The northern boundary of the Proto-Tethys Ocean: constraints from structural analysis and U–Pb zircon geochronology of the North Qinling Terrane. Journal of Asian Earth Sciences 113, 560-574.

Zhou, D., Graham, S.A., 1996. The Songpan-Ganzi complex of the West Qinling Shan as a Triassic remnant ocean basin, in: Yin, A., Harrison, T.M. (Eds.), The Tectonic Evolution of Asia. Cambridge University Press, Cambridge, UK, pp. 442–483.

Zhu, D.C., Wang, Q., Cawood, P.A., Zhao, Z.D., Mo, X.X., 2017. Raising the Gangdese mountains in southern Tibet. Journal of Geophysical Research: Solid Earth 122, 214-223.

Zhu, X.-Y., Chen, F., Li, S.-Q., Yang, Y.-Z., Nie, H., Siebel, W., Zhai, M.-G., 2011. Crustal evolution of the North Qinling terrain of the Qinling Orogen, China: evidence from detrital zircon U–Pb ages and Hf isotopic composition. Gondwana Research 20, 194-204.

Figure captions

Fig. 1 Flowchart showing the integrated method proposed here to aid understanding and interpretation of source-to-sink relationships of basin (including key definitions, plots and step-by-step methods) (a) source unmixing of detrital zircon geochronological data; (b) paleo-elevation estimates of intermediate-composition magmatic rocks of neighboring crustal units.

Fig. 2 Distribution of the major continental and smaller microcontinental blocks in China and adjacent areas (modified after Li et al., 2018). The Songpan-Ganzi basin is highlighted. Yellow labels mark the general positions of proto-source candidates: (1) North China Block (NCB); (2) North Qaidam Block (NQB); (3) South China Block (SCB); (4) North Qinling Belt (NQB); (5) East Kunlun Orogenic Belt (EKOB); (6) North Qiangtang Block (QB); (7) Yidun Terrane (YT); (8) western Southern Qinling Belt (WSQB); (9) eastern Southern Qinling Belt (ESQB); (10) East Kunlun magmatics (EKM); (11) Qinling magmatics (QLM); (12) Qiangtang magmatics (QTM). In addition, red and black bold lines mark sutures and major faults between the continental and microcontinental blocks. 1-Mianlue-A'nyemaqen-Kunlun Suture; 2-Jinshajiang Suture; 3-Longmenshan Fault; 4-Luonan-Luanchuan Fault; 5-Shangdan Suture; 6-Longmu Co-Shuanghu Suture; 7-Banggong Co-Nujiang Suture.

Fig. 3 Alternative tectonic hypotheses for the Songpan-Ganzi basin. (a) Syn-collisional or remnant ocean basin hypothesis (Zhou and Graham, 1996; Nie et al., 1994; Weislogel et al., 2006; Wang et al., 2016). This is revised to include the probable South China Block affinity of the Songpan-Ganzi Basin basement (e.g., Wang et al., 2016; Wu et al., 2019); (b) Back-arc basin hypothesis associated with rifting of the Yidun Terrane from Qinling, driven by rollback of Paleotethyan oceanic lithosphere (e.g., Klimetz, 1983; Gu, 1994; Pullen et al., 2008; Ding et al., 2013). Abbreviations: AS, A’nyemaqen-Kunlun Suture; SS, Shangdan Suture; MS, Mianlue Suture; LS, Longmen Shan Thrust; GS, Ganzi-Litang Suture; JS, Jinshajiang Suture.

Fig. 4 Tectonic map showing the major terranes, suture zones and the Songpan-Ganzi basin (modified after Ding et al., 2013). Locations of the newly analyzed samples (n=7) are highlighted, together with the general positions for the compiled data. Blue dashed lines mark the boundaries of the Songpan-Ganzi basin. Blue labels mark the general positions of potential sources: (1) North China Block (NCB); (2) North Qaidam Block (NQB); (3) South China Block (SCB); (4) East Kunlun Orogenic Belt (EKOB); (5) North Qiangtang Block (QB); (6) Yidun Terrane (YT); (7) western Southern Qinling Belt (WSQB); (8) East Kunlun magmatics (EKM); (9) Qiangtang magmatics (QTM). See Figure 2 for detailed proto-source locations.

Fig. 5 Restored Triassic isopachs of the Songpan-Ganzi basin based on Source Parameter Imaging (Zhang et al., 2019). Paleocurrent data are shown in black arrows (Weislogel et al., 2006; Ding et al., 2013; Jian et al.,2019). General locations of the northeastern (a), southeastern (b), central (c) and western (d) depocenters are highlighted. Blue labels mark the general positions of potential sources: (1) North China Block (NCB); (2) North Qaidam Block (NQB); (3) South China Block (SCB); (4) East Kunlun Orogenic Belt (EKOB); (5) North Qiangtang Block (QB); (6) Yidun Terrane (YT); (7) western Southern Qinling Belt (WSQB); (8) East Kunlun magmatics (EKM); (9) Qiangtang magmatics (QTM). See Figure 2 for detailed proto-source locations.

Fig. 6 Kernel density estimate (KDE) plots of U-Pb ages of detrital zircon from the

newly analyzed Triassic sandstones of the Songpan-Ganzi basin and related sources. Vertical color bars indicate common peaks associated with specific orogenic events and regions. The detrital zircon age range of ~2600-2400 Ma is related to the crustal growth and cratonization in the North China Block (Zhao et al., 2005; Wang et al., 2017), the age range of ~2000-1600 Ma is related to the orogenesis and subsequent rifting magmatism in the North China Block (Zhai, 2010), the age range of 1000-700 Ma is related to the amalgamation and breakup of the Rodinia supercontinent (Wang and Li, 2003; Zhao et al., 2011), the age range of 500-360 Ma and 300-200 Ma are primarily related to the subduction and continental collision of Prototethys and Paleotethys, respectively (Li et al., 2018; Dong et al., 2018; Hu et al., 2020a; Wu et al., 2020). The North China Block data are from Kröner et al. (1988), Darby and Gehrels (2006), Xia et al. (2006a, 2006b), Tung et al. (2007), Li et al. (2008), Liu et al. (2011) and Wan et al. (2011b); the North Qaidam Block data are from Sun et al. (2019, 2022), and references therein; the South China Block data are from Liu et al. (2008), Sun et al. (2008, 2009), Wang et al. (2010, 2012, 2013); the North Qinling Belt data are from Diwu et al. (2010, 2014), Wan et al. (2011a), Zhu et al. (2011), Shi et al. (2013), Zhang et al. (2015) and Zhao et al. (2015); the western South Qinling Belt data are from Chen et al. (2010), Wu et al. (2012), Wang et al. (2014) and Yan et al. (2016a); the eastern South Qinling Belt data are from Duan (2010), Ling et al. (2010), Dong et al. (2013) and Yan et al. (2016b); the East Kunlun Orogenic Belt data are from Huang et al. (2017) and Wu et al. (2019); the North Qiangtang Block data are from Pullen et al. (2008), Gehrels et al. (2011) and He et al. (2011); the Yidun Terrane data are from Reid et al.

(2007) and Tian et al. (2020); the Qinling magmatics data are from Hu et al. (2020b), and references therein; the East Kunlun magmatics data are from Dong et al. (2018) and references therein; finally the Qiangtang magmatics data are from Lu et al. (2019) and references therein.

Fig. 7 Non-metric multidimensional scaling (MDS) plot comparing the detrital zircon age component older than 227 Ma from the Songpan-Ganzi basin. The MDS plot compares the >227 Ma age component of individual samples from the Songpan-Ganzi basin. Two unique similarity clusters are apparent in the MDS plot. One cluster indicates similarity between the Songpan-Ganzi basin sediments and the major continent blocks (North China Block, South China Block, North Qaidam, North Qiangtang Block, North Qinling Belt and the western South Qinling Belt). A second cluster indicates similarity between the sandstones and the Qiangtang, Kunlun and Qinling magmatics.

Fig. 8 Non-metric multi-dimensional scaling (MDS) maps (based on Kuiper distance) of detrital zircon U-Pb ages of samples compiled for the (a) northeastern, (b) southeastern, (c) central (c) and (d) western depocenters of the Songpan-Ganzi basin. Data from this study, and from Bruguier et al. (1997), Weislogel et al. (2006), Ding et al. (2013) and Jian et al. (2019) are compiled. The maps were constructed using 'Provenance'-an R package for statistical provenance analysis (Vermeesch et al., 2016).

Fig. 9 Example of model results of group 3 samples (2004T069, 18MK37, 18BPG20 and 18SGN07) from the northeastern depocenter of the Songpan-Ganzi basin. Sources: 1-North China Block; 2-North Qaidam Block; 3-South China Block; 4-North Qinling Belt; 5-East Kunlun Orogenic Belt; 6-North Qiangtang Block; 7-Yidun Terrane; 8-western Southern Qinling Belt; 9-eastern Southern Qinling Belt; 10-East Kunlun magmatics; 11-Qinling magmatics; 12-Qiangtang magmatics.

Fig. 10 Contour map showing the calculated paleo-elevation of the Songpan-Ganzi basin and the surrounding crustal units from Permian-Early Triassic to Late Triassic (Norian-Rhaetian). Black stars refer to the paleo-bathymetry from the fossil record (see Sections 3.2 and 4.2), white stars represent the calculated paleo-elevations of the magmatic rocks (Supplementary Tables S3-S4). Paleocurrent data, shown as black arrows, are from Weislogel et al. (2006), Ding et al. (2013) and Jian et al. (2019). Blue labels mark the general positions of proto-source candidates: (1) North China Block (NCB); (2) North Qaidam Block (NQB); (3) South China Block (SCB); (4) North Qinling Belt (NQB); (5) East Kunlun Orogenic Belt (EKOB); (6) North Qiangtang Block (QB); (7) Yidun Terrane (YT); (8) western Southern Qinling Belt (WSQB); (9) eastern Southern Qinling Belt (ESQB); (10) East Kunlun magmatics (EKM); (11) Qinling magmatics (QLM); (12) Qiangtang magmatics (QTM). Faults: 1-Shangdan Suture; 2-Mianlue-Anemaqen Suture; 3-Jinshajiang Suture; 4-Longmu Co-Shuanghu Suture; 5-Longmenshan Fault.

Graphical Abstract

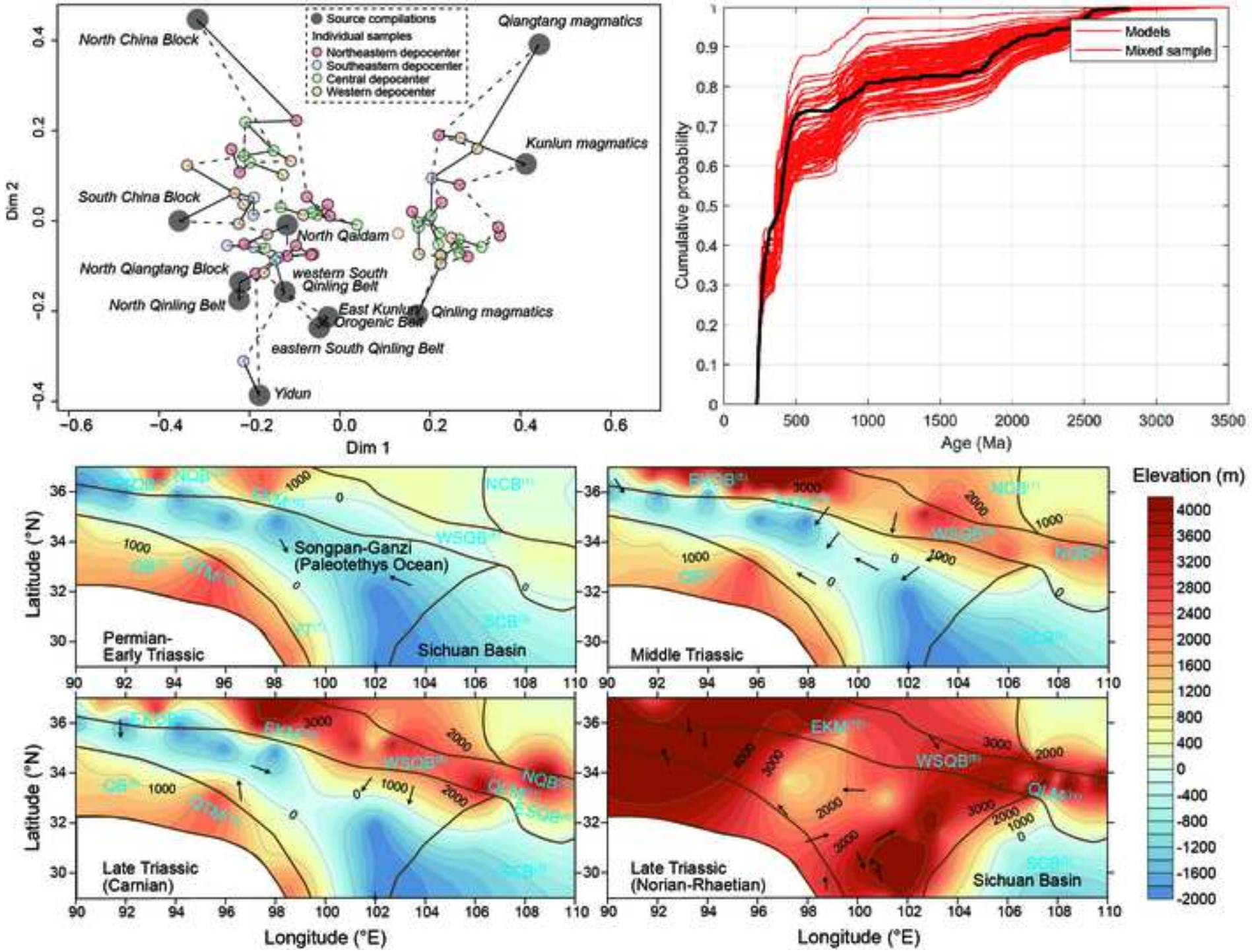

- A combined method is proposed to help reconstruct source-to-sink sediment transport
- Source proportions are tested using simulations of detrital zircon age populations
- Paleo-elevation calculations of adjacent blocks shed light on sediment provenance
- The method leads to a new interpretation of sediment sources, supply and deposition

Figure 1

Click here to access/download;Figure;Figure 1.jpg

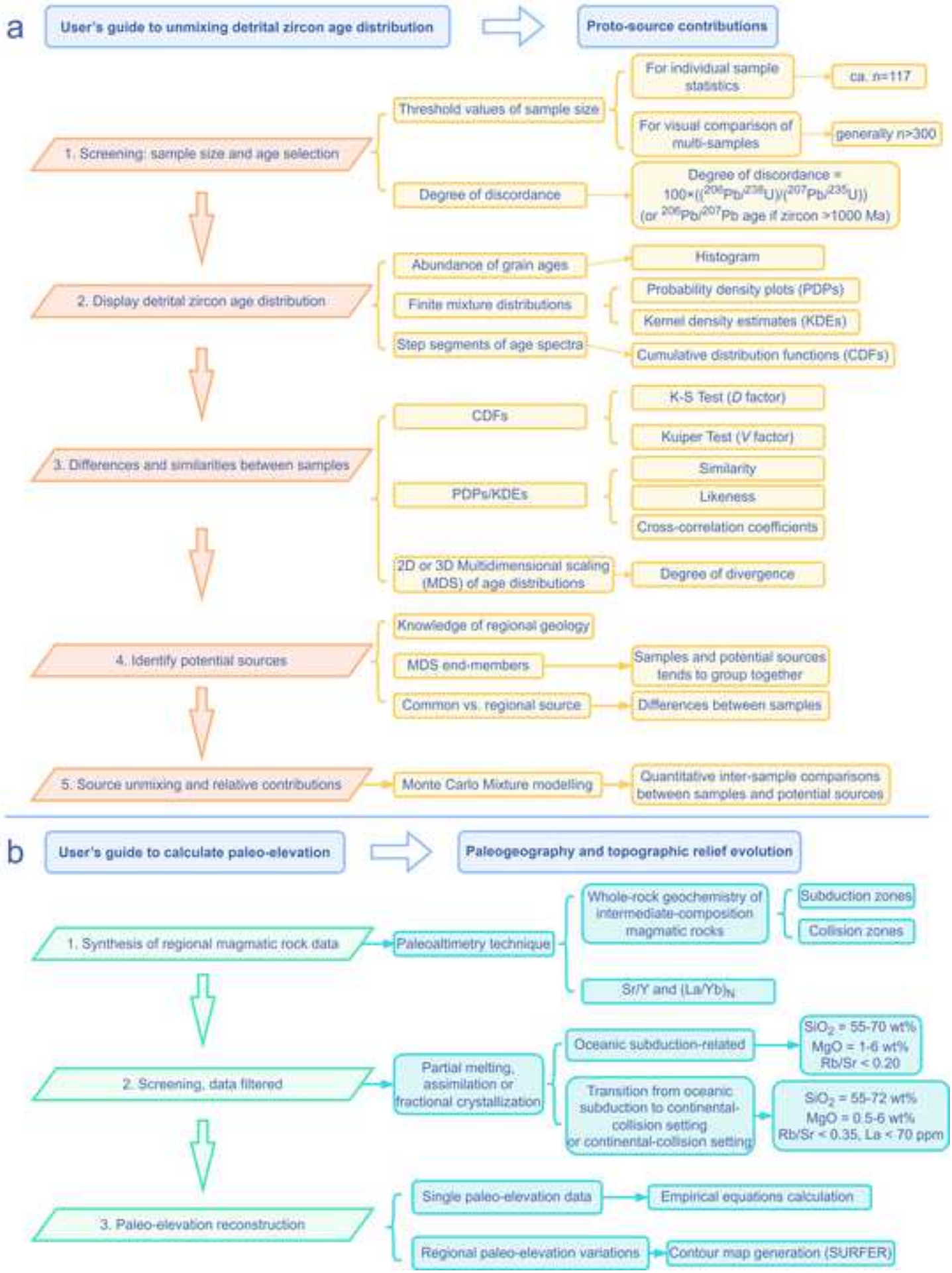

Figure 2

Click here to access/download;Figure;Figure 2.jpg

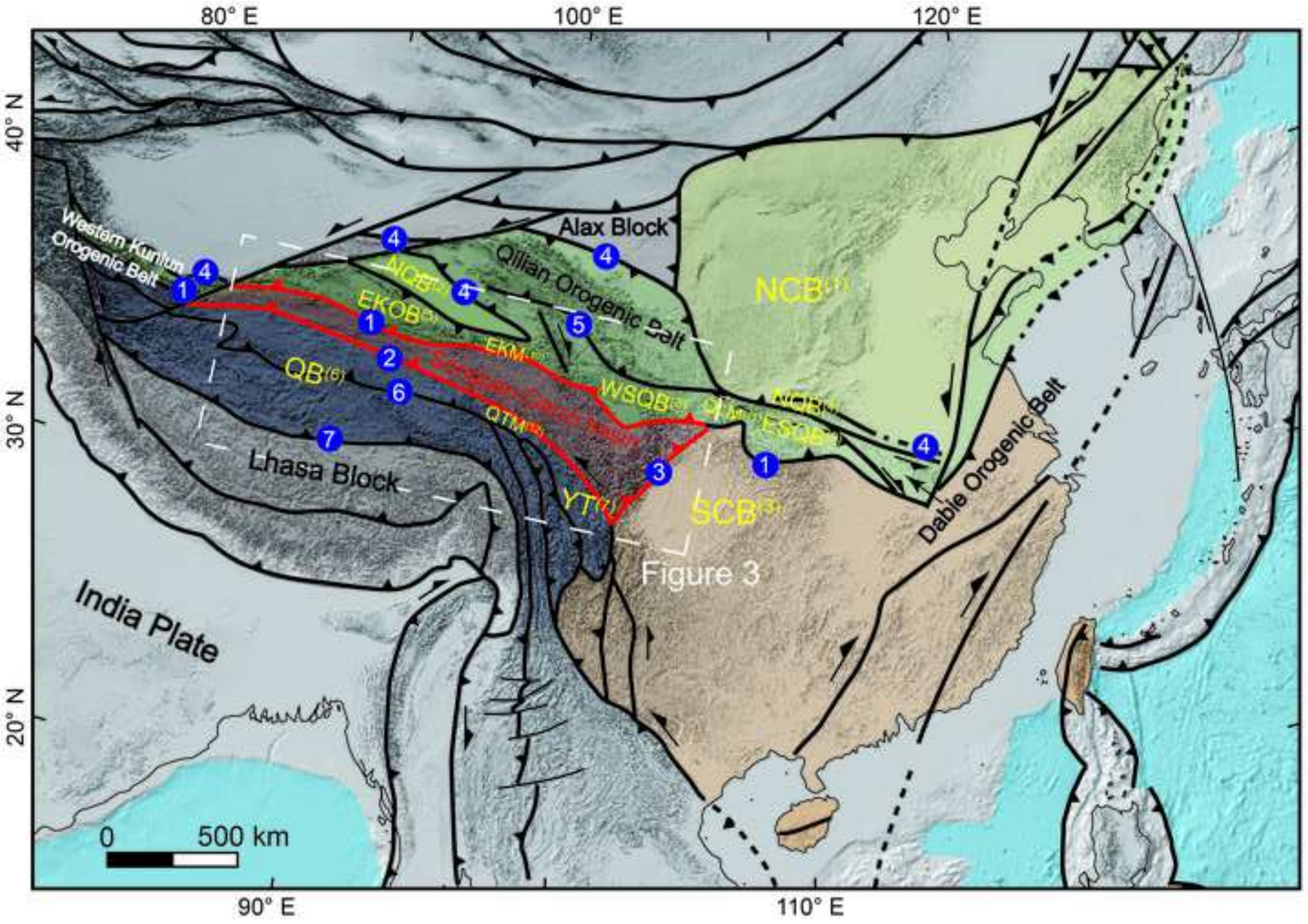

Figure 3



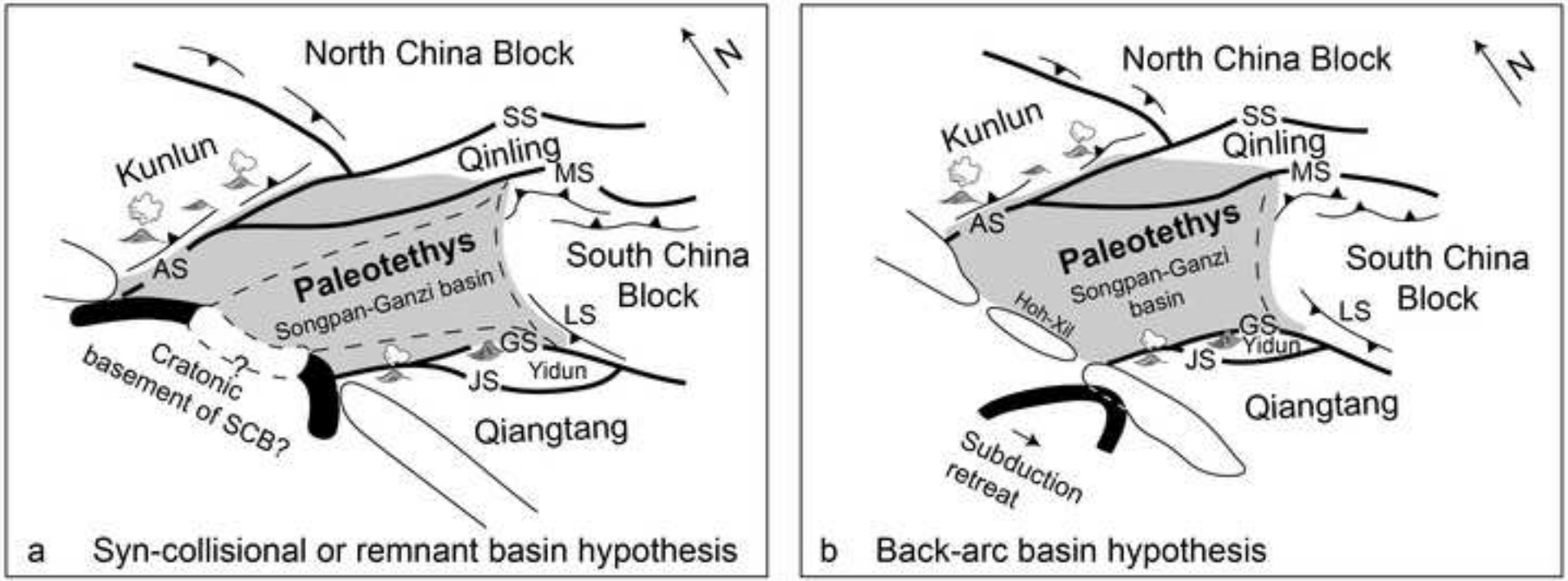

Figure 4

Click here to access/download;Figure;Figure 4.jpg

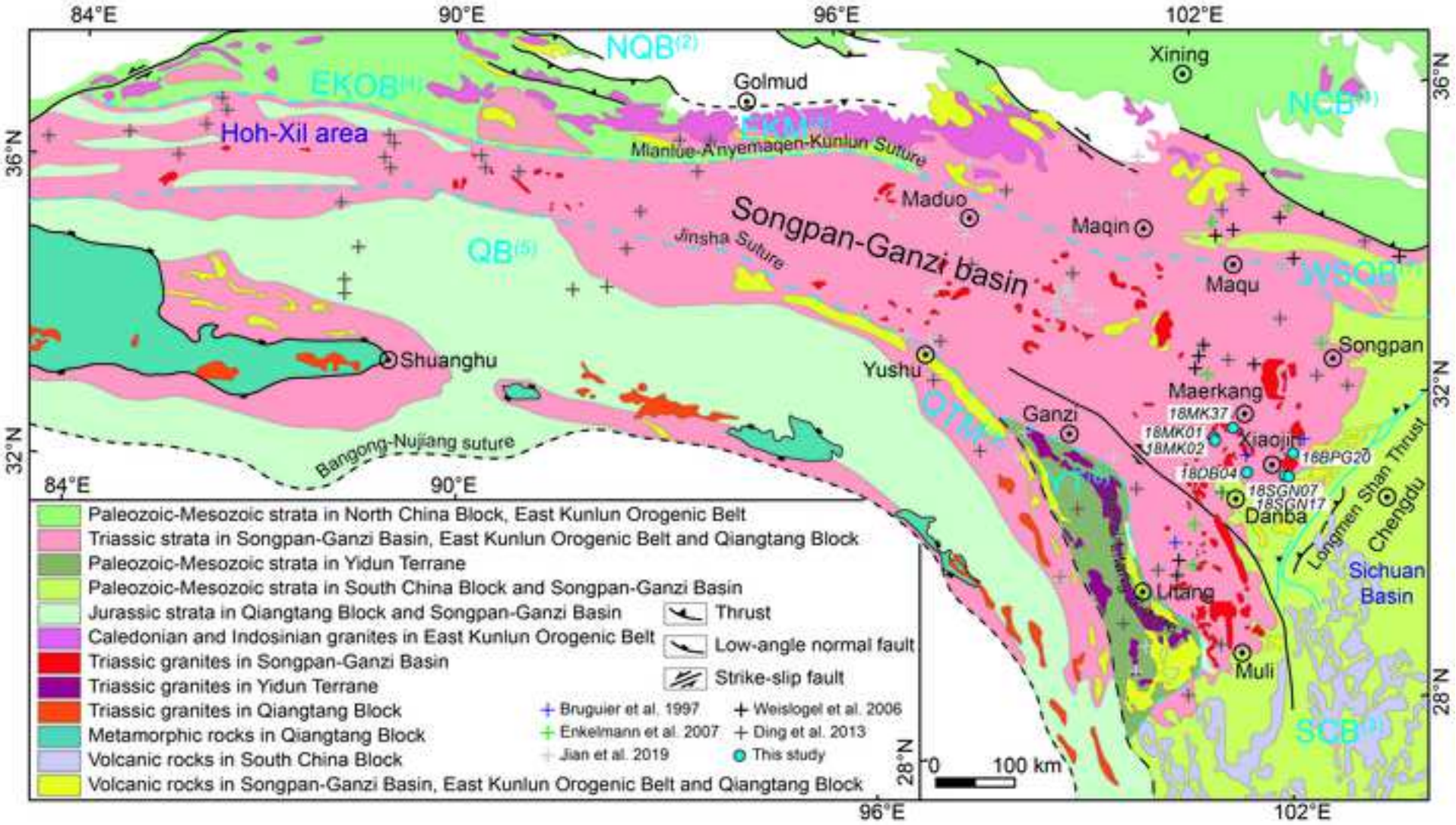

Figure 5

Click here to access/download;Figure;Figure 5.jpg

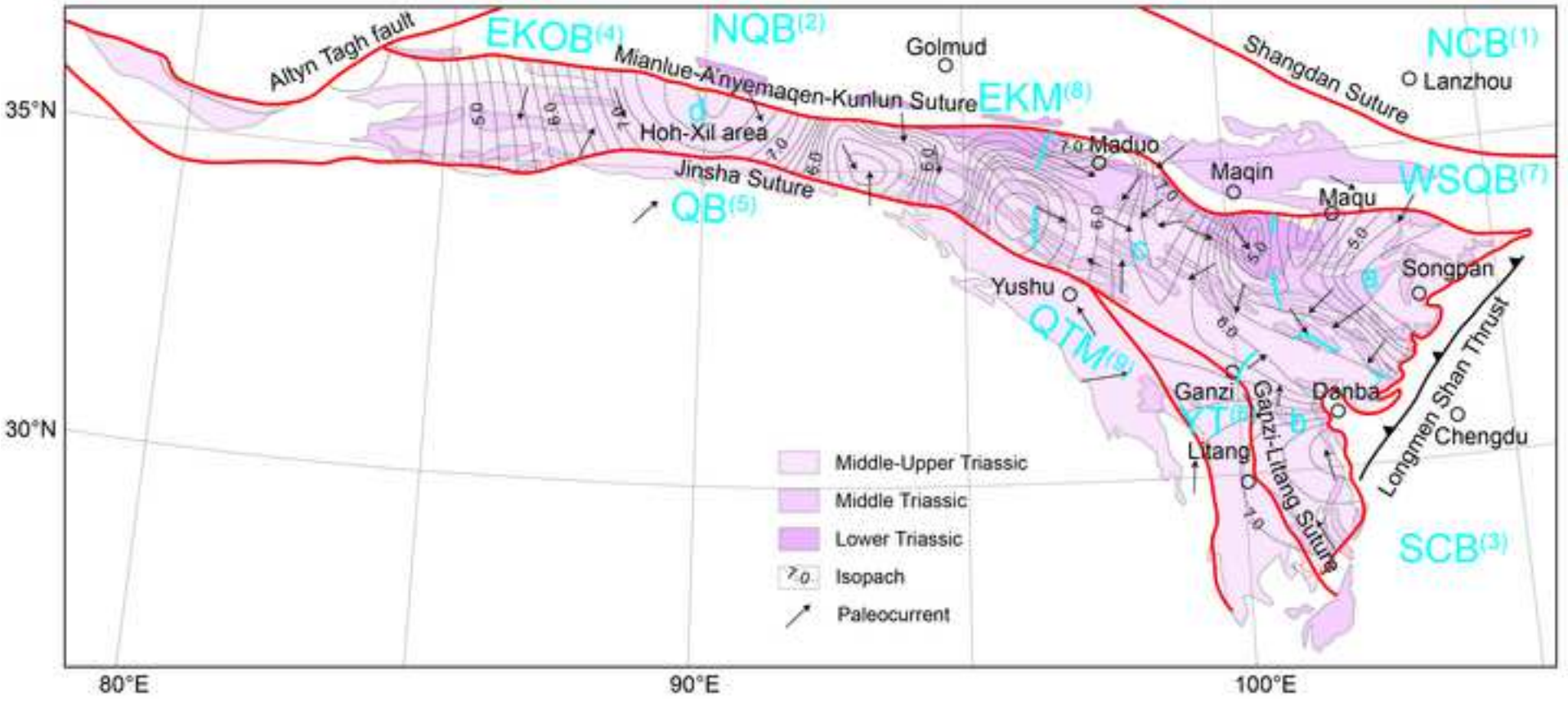

Figure 6

Click here to access/download;Figure;Figure 6.jpg

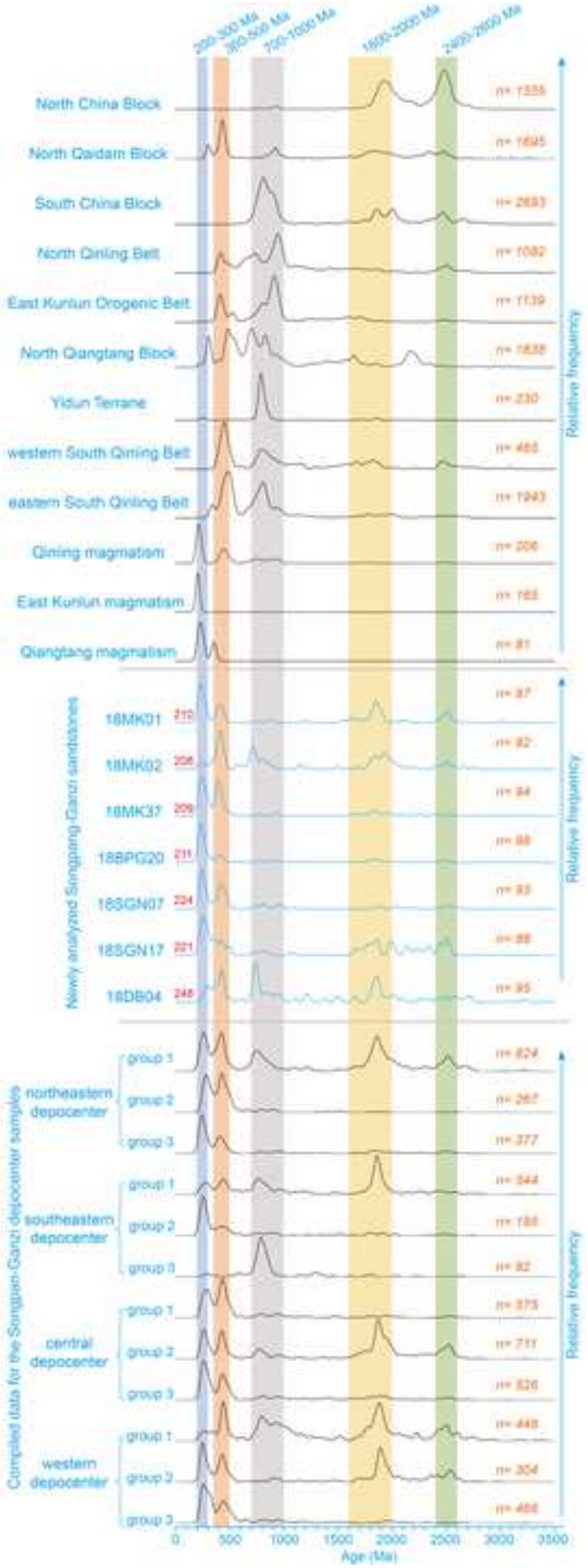

Figure 7

Click here to access/download;Figure;Figure 7.jpg

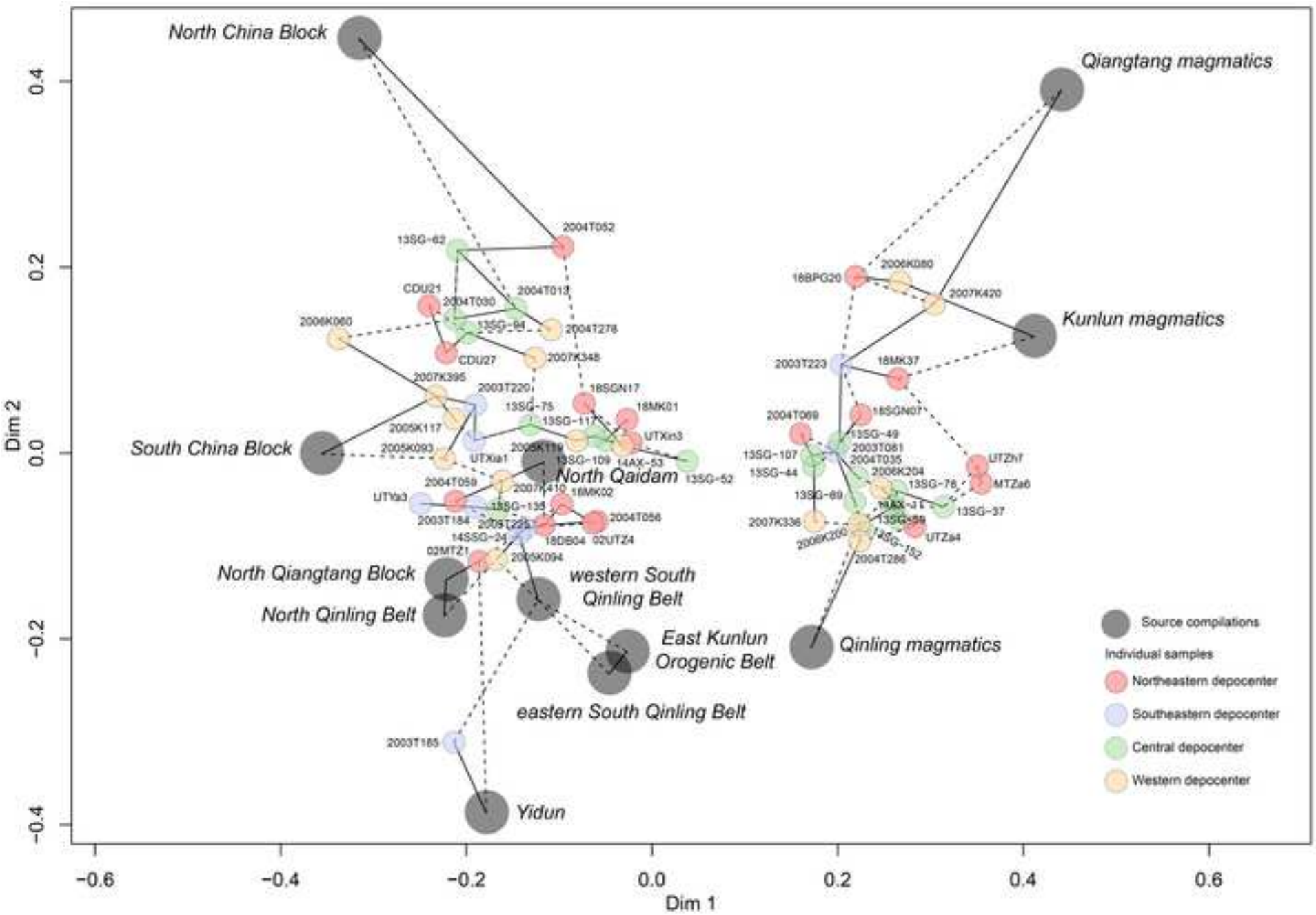

Figure 8

Click here to access/download;Figure;Figure 8.jpg

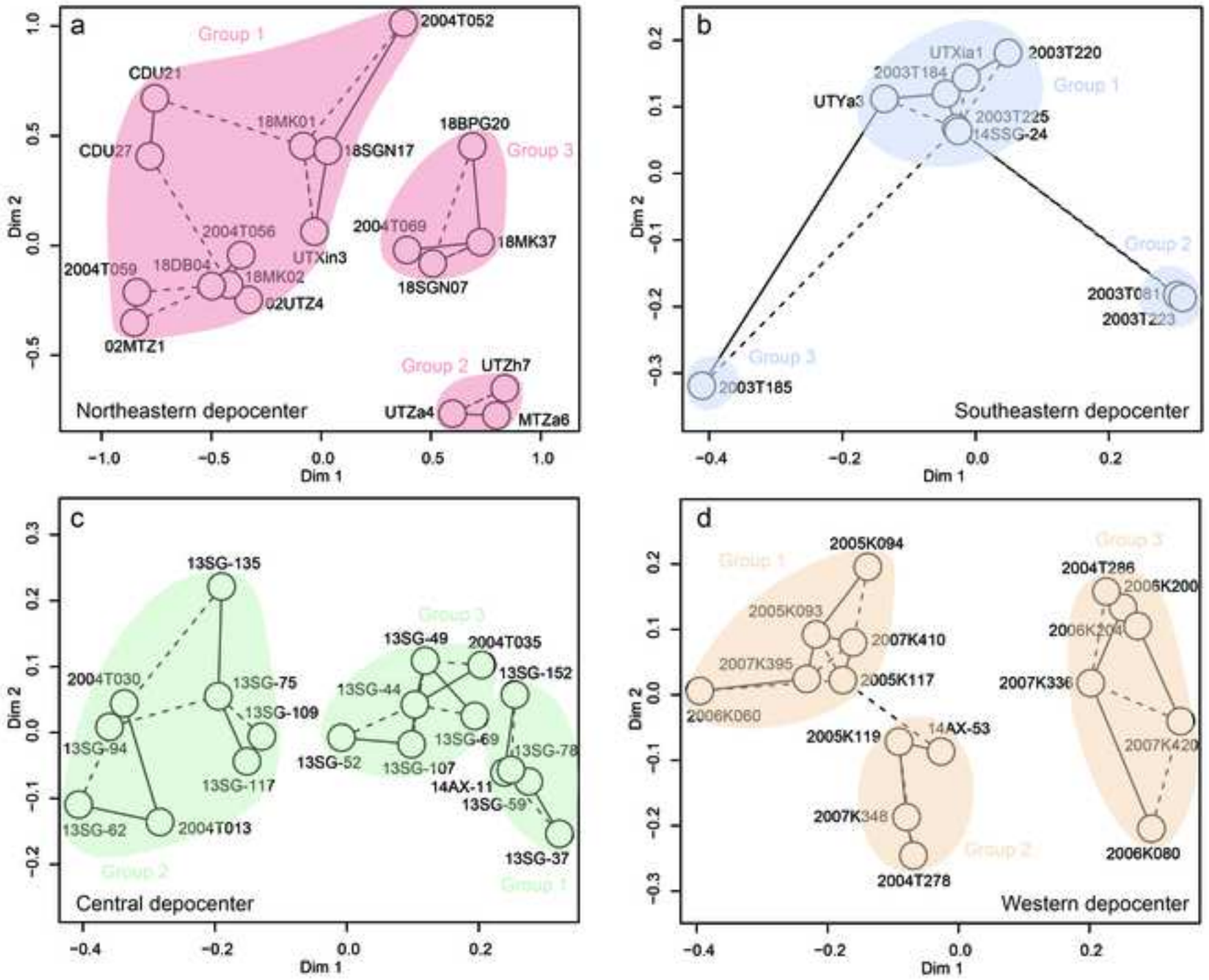

Figure 9

Click here to access/download;Figure;Figure 9.jpg

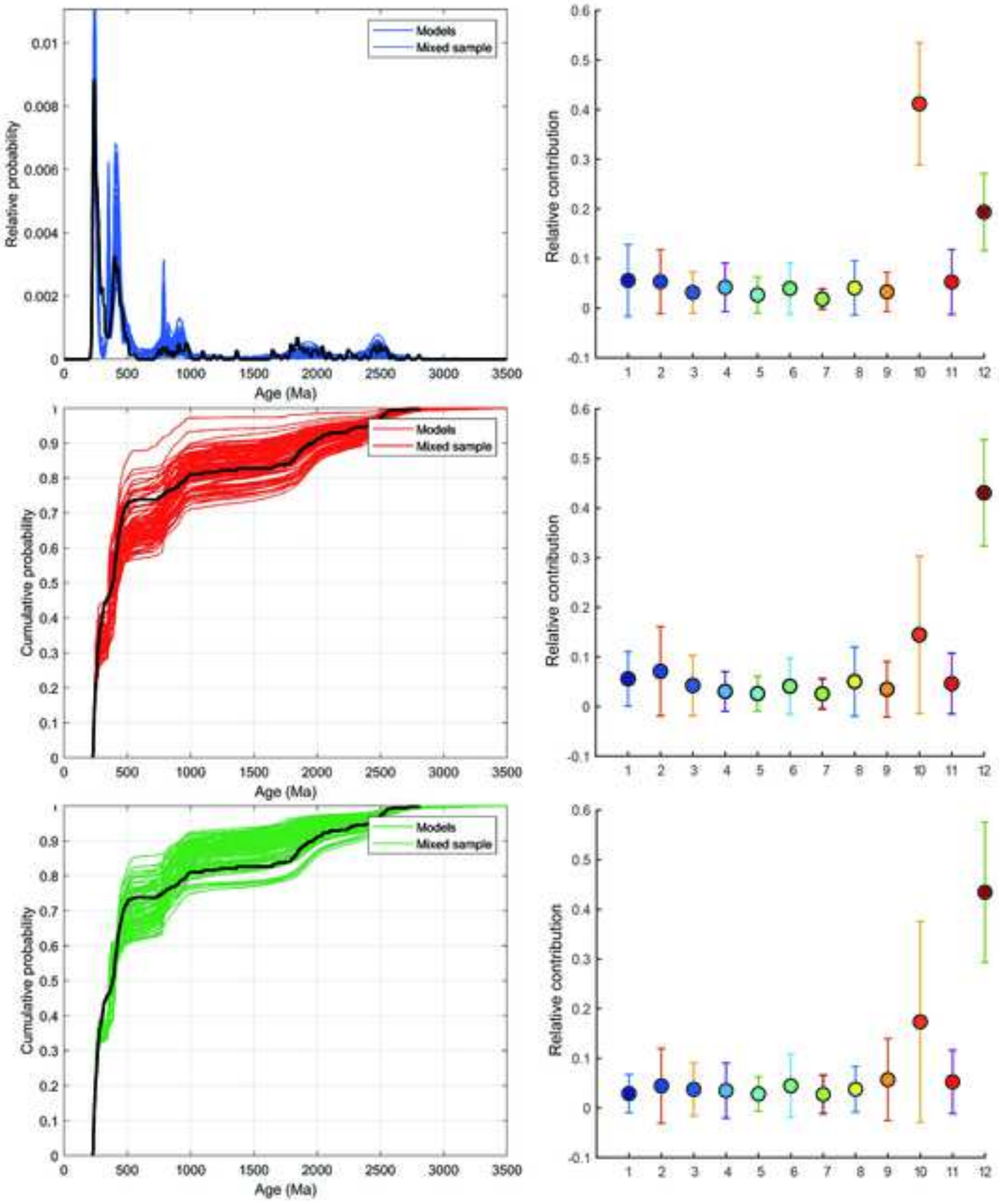

Figure 10

Click here to access/download;Figure;Figure 10.jpg

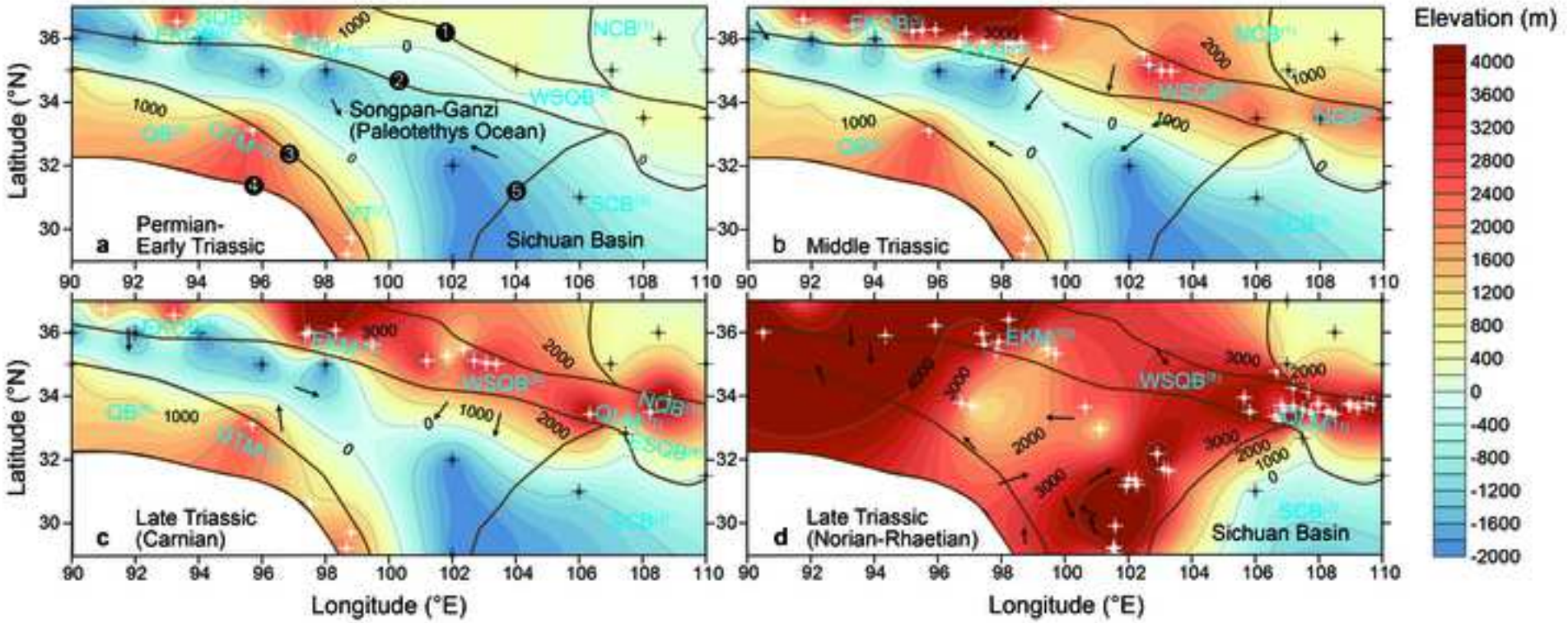

Table 1 Model results showing source contributions (%) based on cross-correlation coefficient (top row), Kuiper test V statistic (middle row) and K-S test D statistic (bottom row)

| | | Cratonic basement (detrital zircon) | | | | | | | | | Magmatics (igneous zircon) | | | Comparison me | |
|---|---|---|---|---|---|---|---|---|---|---|---|---|---|---|---|
| Depocenter | Subgroup | North China Block | North Qaidam Block | South China Block | North Qinling Belt | East Kunlun Orogenic Belt | North Qiangtang Block | Yidun Terrane | western South Qinling Belt | eastern South Qinling Belt | East Kunlun | Qinling | Qiangtang | $R^2$ | V |
| northeastern depocenter | NE-G1 | 18.24 | 30.31 | 7.46 | 4.19 | 3.91 | 4.68 | 1.91 | 5.95 | 3.42 | 7.35 | 4.31 | 8.26 | | |
| | NE-G1 | 19.29 | 32.79 | 5.22 | 4.71 | 4.48 | 4.37 | 2.67 | 4.47 | 3.45 | 7.15 | 3.61 | 7.78 | 0.571 | 0.124 |
| | NE-G1 | 21.35 | 24.24 | 7.10 | 4.91 | 4.89 | 4.90 | 2.68 | 5.17 | 3.63 | 9.76 | 4.50 | 6.87 | | |
| | NE-G2 | 2.14 | 39.69 | 1.58 | 2.34 | 16.00 | 3.86 | 0.98 | 4.23 | 6.27 | 8.69 | 7.00 | 7.22 | | |
| | NE-G2 | 0.69 | 2.41 | 1.41 | 1.83 | 5.69 | 1.50 | 1.50 | 2.23 | 4.61 | 67.87 | 5.38 | 4.89 | 0.569 | 0.342 |
| | NE-G2 | 1.61 | 5.68 | 1.96 | 2.87 | 7.82 | 3.24 | 2.22 | 3.38 | 8.13 | 43.14 | 10.37 | 9.60 | | |
| | NE-G3 | 5.31 | 4.69 | 3.81 | 4.35 | 3.42 | 3.77 | 1.89 | 4.07 | 2.78 | 42.20 | 4.15 | 19.57 | | |
| | NE-G3 | 6.41 | 6.78 | 4.04 | 3.12 | 2.86 | 3.43 | 2.54 | 4.31 | 3.50 | 15.86 | 5.32 | 41.84 | 0.809 | 0.175 |
| | NE-G3 | 4.71 | 5.02 | 3.13 | 2.59 | 4.36 | 3.43 | 3.03 | 4.68 | 4.41 | 13.35 | 4.87 | 46.43 | | |
| southeastern depocenter | SE-G1 | 14.16 | 24.19 | 22.09 | 3.85 | 3.16 | 6.97 | 2.10 | 9.64 | 5.82 | 2.16 | 3.02 | 2.84 | | |
| | SE-G1 | 15.81 | 26.92 | 11.75 | 8.48 | 4.09 | 9.77 | 3.03 | 12.71 | 2.70 | 1.34 | 2.06 | 1.34 | 0.352 | 0.188 |
| | SE-G1 | 13.59 | 23.75 | 10.74 | 9.33 | 5.96 | 8.12 | 4.18 | 11.08 | 5.00 | 2.59 | 3.26 | 2.41 | | |
| | SE-G2 | 5.02 | 8.23 | 3.32 | 3.73 | 4.05 | 3.89 | 1.74 | 4.22 | 4.07 | 24.56 | 5.64 | 31.53 | | |
| | SE-G2 | 2.37 | 5.94 | 3.78 | 2.61 | 4.01 | 3.27 | 3.03 | 4.44 | 3.67 | 7.95 | 2.90 | 56.04 | 0.597 | 0.225 |
| | SE-G2 | 3.42 | 5.41 | 3.65 | 3.56 | 3.53 | 4.84 | 4.22 | 3.72 | 4.19 | 13.26 | 4.34 | 45.85 | | |
| | SE-G3 | 1.18 | 1.54 | 69.15 | 3.51 | 1.94 | 4.41 | 5.94 | 2.62 | 4.51 | 1.40 | 2.40 | 1.41 | | |
| | SE-G3 | 2.31 | 2.89 | 5.92 | 6.69 | 4.24 | 7.12 | 56.78 | 3.08 | 4.07 | 1.92 | 3.26 | 1.72 | 0.693 | 0.220 |
| | SE-G3 | 2.19 | 3.57 | 4.68 | 7.62 | 4.27 | 7.46 | 56.31 | 3.89 | 4.44 | 1.35 | 2.66 | 1.57 | | |
| central depocenter | C-G1 | 1.98 | 48.65 | 1.80 | 3.73 | 8.37 | 2.82 | 1.11 | 4.45 | 5.36 | 10.52 | 5.36 | 5.85 | | |
| | C-G1 | 1.42 | 5.02 | 1.72 | 2.96 | 8.05 | 3.52 | 2.70 | 2.71 | 5.23 | 50.09 | 6.61 | 9.97 | 0.683 | 0.222 |
| | C-G1 | 2.20 | 8.46 | 2.37 | 3.49 | 11.84 | 3.60 | 2.58 | 6.92 | 5.03 | 37.70 | 7.14 | 8.67 | | |
| | C-G2 | 38.19 | 18.17 | 4.99 | 3.28 | 3.52 | 4.68 | 1.28 | 4.85 | 3.76 | 8.28 | 4.79 | 4.21 | | |
| | C-G2 | 39.58 | 17.08 | 5.33 | 4.52 | 4.16 | 5.49 | 2.12 | 5.32 | 4.87 | 3.72 | 3.48 | 4.35 | 0.513 | 0.168 |
| | C-G2 | 33.55 | 20.42 | 5.31 | 3.90 | 4.06 | 4.72 | 3.13 | 5.42 | 4.28 | 5.95 | 4.24 | 5.02 | | |
| | C-G3 | 3.53 | 26.76 | 2.73 | 3.97 | 6.39 | 3.58 | 1.19 | 5.59 | 5.80 | 20.43 | 5.48 | 14.58 | | |
| | C-G3 | 2.29 | 10.36 | 2.84 | 3.40 | 4.73 | 3.04 | 3.05 | 5.03 | 5.41 | 15.14 | 4.06 | 40.65 | 0.597 | 0.195 |
| | C-G3 | 3.27 | 11.80 | 3.63 | 5.51 | 5.55 | 4.73 | 2.98 | 4.60 | 5.33 | 23.01 | 4.56 | 25.01 | | |
| western depocenter | W-G1 | 21.34 | 16.45 | 14.91 | 9.00 | 6.41 | 7.44 | 1.76 | 11.99 | 4.42 | 1.55 | 3.29 | 1.44 | | |
| | W-G1 | 20.15 | 18.10 | 7.72 | 18.29 | 4.66 | 10.30 | 2.24 | 11.31 | 2.57 | 1.26 | 1.90 | 1.51 | 0.669 | 0.149 |
| | W-G1 | 25.45 | 12.78 | 9.73 | 14.00 | 5.58 | 9.03 | 2.61 | 11.61 | 3.31 | 1.90 | 2.37 | 1.62 | | |
| | W-G2 | 32.71 | 14.85 | 3.40 | 3.10 | 3.91 | 3.90 | 1.15 | 3.57 | 3.29 | 19.20 | 4.49 | 6.44 | | |
| | W-G2 | 37.40 | 9.53 | 4.22 | 3.09 | 3.95 | 3.80 | 2.07 | 4.54 | 3.68 | 12.17 | 4.30 | 11.25 | 0.588 | 0.159 |
| | W-G2 | 32.93 | 10.91 | 5.10 | 3.83 | 4.81 | 4.42 | 2.50 | 5.08 | 3.58 | 11.83 | 4.68 | 10.33 | | |
| | W-G3 | 3.02 | 21.46 | 2.21 | 2.84 | 10.41 | 3.44 | 1.50 | 4.57 | 8.42 | 11.22 | 8.68 | 22.23 | | |
| | W-G3 | 1.37 | 4.35 | 1.68 | 2.73 | 5.53 | 4.50 | 2.14 | 4.10 | 7.53 | 13.41 | 4.86 | 47.80 | 0.580 | 0.238 |
| | W-G3 | 2.91 | 5.15 | 2.84 | 4.14 | 6.96 | 4.75 | 3.23 | 4.14 | 7.24 | 20.07 | 6.72 | 31.85 | | |
| Average | | 12.31 | 14.84 | 7.04 | 4.89 | 5.49 | 4.91 | 5.45 | 5.55 | 4.66 | 14.98 | 4.61 | 15.28 | | |

| thods |
| --- |
| D |
| 0.077 |
| 0.198 |
| 0.111 |
| 0.105 |
| 0.128 |
| 0.132 |
| 0.135 |
| 0.103 |
| 0.113 |
| 0.094 |
| 0.105 |
| 0.137 |

Supplementary tables

**Declaration of interests**

☒The authors declare that they have no known competing financial interests or personal relationships that could have appeared to influence the work reported in this paper.

☐The authors declare the following financial interests/personal relationships which may be considered as potential competing interests: